



Moment tensor inversion of Explosive Long Period events recorded on Arenal Volcano, Costa Rica, constrained by synthetic tests

R. Davi, G.S. O'Brien, I. Lokmer, C.J. Bean, Philippe Lesage, M. Mora

► To cite this version:

R. Davi, G.S. O'Brien, I. Lokmer, C.J. Bean, Philippe Lesage, et al.. Moment tensor inversion of Explosive Long Period events recorded on Arenal Volcano, Costa Rica, constrained by synthetic tests. *Journal of Volcanology and Geothermal Research*, Elsevier, 2010, 194 (4), pp.189-200. <10.1016/j.jvolgeores.2010.05.012>. <hal-00504737>

HAL Id: hal-00504737

<http://hal.univ-smb.fr/hal-00504737>

Submitted on 15 Jul 2014

HAL is a multi-disciplinary open access archive for the deposit and dissemination of scientific research documents, whether they are published or not. The documents may come from teaching and research institutions in France or abroad, or from public or private research centers.

L'archive ouverte pluridisciplinaire **HAL**, est destinée au dépôt et à la diffusion de documents scientifiques de niveau recherche, publiés ou non, émanant des établissements d'enseignement et de recherche français ou étrangers, des laboratoires publics ou privés.

1 **Moment tensor inversion of Explosive Long Period events recorded on Arenal**
2 **Volcano, Costa Rica, constrained by synthetic tests.**

3

4 R. Davi¹, G.S. O'Brien^{1,2}, I. Lokmer^{1,2}, C.J. Bean^{1,2}, P. Lesage³, M.M. Mora.⁴

5

6 ¹Seismology and Computational Rock Physics Laboratory, School of Geological
7 Sciences, University College Dublin, Belfield, Dublin 4, Ireland.

8 ²Complex and Adaptive Systems Laboratory (CASL), University College Dublin,
9 Belfield, Dublin 4, Ireland.

10 ³Laboratoire de Géophysique Interne et Tectonophysique, CNRS, Université de Savoie,
11 73376 Le Bourget-du-Lac Cedex, France

12 ⁴Escuela Centroamericana de Geología, Universidad de Costa Rica, Ciudad Universitaria
13 Rodrigo Facio, San Pedro de Montes de Oca, 214-2060 San José, Costa Rica.

14

15 **Abstract**

16

17 In order to constrain the moment tensor solution of an explosive seismic event recorded
18 on Arenal volcano, Costa Rica, we perform tests using synthetic data. These data are
19 generated using a 3D model including the topography of the volcano and the best
20 estimation of the velocity model available for Arenal. Solutions for (i) the moment tensor
21 components, and (ii) the moment tensor plus single forces, are analysed. When noisy data
22 and mislocated sources are used in the inversion, spurious single forces are easily
23 generated in the solution for the moment tensor components plus single forces. Forces
24 also appear when the inversion is performed using an explosive event recorded on Arenal

25 in 2005. Synthetic tests indicate that these forces might be spurious. However the
26 mechanism is correctly retrieved by the inversion in both solutions. The ability to recover
27 the explosive mechanism for the 2005 event combined with the interpretative aids from
28 the synthetic tests will enable us to invert for the large variation in events observed on
29 Arenal.

30

31 Keywords: Arenal volcano, moment tensor inversion, single forces, synthetic tests

32

33 **1. Introduction**

34

35 Volcanoes are complex and challenging environments showing a great variety of
36 behaviour. A range of earthquake types are regularly recorded on volcanoes. They
37 include: high frequency tectonic-like events, also known as volcano tectonic events,
38 (VT), explosions, long period events (LP) and tremor. VT events have energy in the
39 range of 2-20 Hz with very similar signatures to tectonic earthquakes. They are due to
40 brittle rock failure, generated by regional tectonic forces, dyke propagation or pore over-
41 pressure (McNutt, 2005). LP events and tremor are normally characterized by strongly
42 peaked spectra. Their energy is concentrated between 0.2 and 5 Hz and they are thought
43 to be caused by fluid movements inside volcanic conduits (Chouet, 2003). Since tremor
44 and LP events seem to have common characteristics, differing only in duration, some
45 authors believe they share the same source mechanism (Chouet, 1996; Neuberg et al.,
46 2000). These types of events often precede and accompany volcanic eruptions, hence a
47 deeper knowledge of their source origin may be helpful in volcanic event forecasting.

48 One of the most common tools used to retrieve the seismic source mechanism is a
49 moment tensor inversion. The combination of moment tensor components represents a
50 system of equivalent forces that produces the same wavefield as the actual physical
51 processes at the source. Inverting for the seismic source mechanism has become a
52 common procedure. Inversions for very long period events (VLP) have been successfully
53 performed (Ohminato et al., 1998; Chouet et al., 2003) as the very long wavelengths are
54 not influenced by structural heterogeneities. However, this is not always the case for
55 inversions of LP events. The shortest wavelengths are sensitive to velocity structures and
56 strong topographic effects (Bean et al., 2008; Lokmer et al., 2007; Lokmer et al., 2008;
57 Métaxian et al., 2009). Such effects introduce many uncertainties in the inversion
58 procedure that can lead to apparently stable, but erroneous solutions (Bean et al., 2008).
59 In fact, due to the complexity of volcanic environments (e.g. the lack of sufficient
60 structural information, the high degree of heterogeneity and the scattering effects due to
61 the pronounced topography), it is quite difficult to recover a unique (and correct) source
62 mechanism. The inclusion of single forces in the inversion procedure makes the recovery
63 of the source mechanism an even more challenging task. However, single forces may be
64 common in volcanic environments and have been modelled in other seismic source
65 studies. Takei and Kumazawa (1994) provide a theoretical justification for the physical
66 existence of these forces. However, an accurate quantification of these forces is not
67 available at present. This is due to the fact that an inversion procedure with an increased
68 numbers of free parameters is extremely sensitive to uncertainties in the near-surface
69 velocity model (Bean et al., 2008).
70

71 In this paper, we perform a moment tensor inversion of an explosive event recorded in
72 2005 on Arenal volcano, Costa Rica, using constraints obtained by synthetic tests.
73 Topographical and structural effects are reduced using the best estimation of velocity
74 model available for Arenal volcano and Green's functions are calculated including 15 m
75 resolution digital elevation model of the volcano. In the synthetic tests we assess our
76 ability to retrieve the correct source time function and mechanism when (i) random noise
77 is added to the data, and (ii) the source location is not accurately known. We also
78 investigate how the presence of single forces affects the moment tensor solution. We aim
79 to quantify our ability to accurately recover the true source from real seismic data. The
80 information obtained by performing the synthetic tests is used in the analysis and
81 interpretation of the solution of the inversion performed on real explosion data from
82 Arenal. The methodology used in the calculation of the Green's functions, and in the
83 inversion method, is provided herein. Results of our synthetic tests, the inversion of the
84 real event and the interpretation of the mechanism that generates this event are also
85 presented.

86

87 **2. Arenal volcano**

88

89 Arenal is a small strato-volcano located in north-western Costa Rica and is mainly
90 composed of tephra and lava flows (Soto and Alvarado, 2006); its location and digital
91 elevation model are shown in Figure 1. It was dormant for several centuries until July
92 1968 when a Peléan eruption resulted in 78 fatalities and opened three new craters in the
93 western flank. Arenal's explosive activity is still ongoing today and is preceded, and

94 accompanied, by different types of seismic events. The most common types are LP
95 events, explosions, spasmodic and harmonic tremor, rockfalls and sporadic volcano
96 tectonic swarms (Alvarado and Barquero, 1997). Explosions and LP events have the
97 same frequency range (1-3 Hz), but differ in amplitude. Explosions have larger
98 amplitudes and are accompanied by a large, audible air-shock. The explosion coda often
99 evolves into tremor (Hagerty et al., 2000). Tremor is the most common type of event at
100 Arenal with a duration that can last for several hours and comprises spasmodic and
101 harmonic. Harmonic tremor can be distinguished from spasmodic tremor by their
102 regularly spaced frequency peaks with most of the energy concentrated between 0.9 and 2
103 Hz. Spasmodic tremor energy spans 1-6 Hz. There is no clear difference in the genesis of
104 spasmodic and harmonic tremor; the former can progressively evolve into the latter and
105 vice-versa (Lesage et al., 2006). Most of the tremor exhibits a progressive gliding in
106 frequency that can last tens to hundreds of seconds. The gliding phenomenon can be
107 generated by pressure changes in the fluid inside the conduit (Hagerty et al., 2000). The
108 number of seismic events can be variable during the day. However, in recent decades a
109 decrease in the number and amplitude of explosions has been recognised (Lesage et al.,
110 2006). Arenal's seismicity is often accompanied by gas emissions produced during the
111 explosions and by passive degassing in rhythmic pulses along the edge of the crater
112 (William-Jones et al., 2001). The origin of these seismic events is, at present, not fully
113 understood.

114

115 **3. Methodology**

116

117 The elastic Green's functions are defined as the Earth's response to an impulsive source
118 generated at a certain point (source location) and propagating to a receiver location in an
119 elastic Earth. The n^{th} -component of the displacement, recorded at position \mathbf{x} and time t ,
120 can be written as (Aki and Richards, 2002):

121

$$122 \quad u_n(\mathbf{x}, t) = M_{pq}(t) * G_{np,q}(\mathbf{x}, t) + F_p(t) * G_{np}(\mathbf{x}, t), \quad n, p, q = 1, 2, 3 \quad (1)$$

123

124 where M_{pq} is the force couple or dipole in the pq direction acting at the source, F_p is the
125 single force acting in the p direction, and G_{np} and $G_{np,q}$ represent the n^{th} components of
126 the corresponding medium responses (Green's functions) and their derivatives,
127 respectively. The asterisk indicates convolution and the summation convention applies.

128 Volcanoes are the most "promising" environments in which single forces are likely to be
129 found (Takei and Kumazawa, 1994), even if the existence of these single forces in the LP
130 process is, at present, not reliably constrained by experiments or observations. For VLP
131 events, Chouet (2003) attributes single forces to gravitational energy in the source
132 volume due to the ascent of a slug of gas in the volcanic conduit or by a volcanic jet
133 during an explosion. The latter phenomenon was also successfully modelled using single
134 forces in the recent work of Jolly et al. (2010). The reliability of the inversion results are
135 strongly dependent on the accuracy with which the Green's functions are calculated
136 (Lokmer, 2008). In the past, due to computational restrictions, Green's functions were
137 calculated only for a homogeneous half-space excluding topography. This approach leads
138 to misinterpretations because the seismic wavefield is sensitive to layered velocity
139 models and strongly affected by topographical scattering (Bean et al., 2008). However, in

140 the past decade, topography has been included in the calculation of Green's functions
141 (Ohimanto and Chouet, 2007; Neuber and Pointer, 2000; Jousset et al., 2004; Jolly et al,
142 2010). To avoid incorrect interpretations we require detailed information about the
143 medium i.e. a precise velocity model or near-accurate Green's functions relative to the
144 frequencies of interest. At present, detailed velocity models with structural information,
145 particularly related to the layers close to the surface, are extremely rare on volcanoes due
146 to the considerable cost and effort involved in producing such high resolution velocity
147 models. Therefore, synthetic tests provide a powerful tool for constraining the inversion
148 results and improving the reliability of such interpretations.

149

150 To calculate the Green's functions we use 3D-full wavefield numerical simulations
151 including topography and the "best" estimate of the velocity structure retrieved from
152 sounding using the spatial autocorrelation (SPAC) method, Métaxian et al., 1997, and
153 seismic refraction experiments carried out on Arenal in 1997 (Mora et al., 2006). In this
154 study, we use the 3D Elastic Lattice Method (ELM), to simulate wave propagation in the
155 elastic medium (O'Brien and Bean, 2004). To calculate the Green's functions we use a 1-
156 D velocity model (Figure 2). This velocity model comprises two major layers following
157 the profile of the topography above a half space medium with velocities of 3.5 km/s for
158 the P-waves (V_p) and 2.0 km/s for the S-waves (V_s) and a maximum density equal to
159 2500 kg/m^3 . The numerical domain consists of a $13 \times 11 \times 6 \text{ km}^3$ space where topography
160 is derived from the Digital Elevation Model (DEM) of the volcano using a spatial grid
161 step of 15 m. Long wavelengths are simulated using a model of large extent with
162 relatively small grid-step. Absorbing boundaries, 900 m thick, are included in the model

163 to avoid edge reflections and ensure the absorption of the longest wavelengths. The top
164 boundary of the model is a free surface including topography. To calculate the Green's
165 functions library for a large number of source locations within a predefined source
166 region, we adopt the Reciprocity Theorem (e.g. Aki and Richards, 2002). Green's
167 functions are calculated over a volume (480 x 300 x 840 m³) of 4735 points located under
168 the crater summit. In addition to calculating the Green's functions for each single point
169 source, we also required their spatial derivatives around the source position. Spatial
170 derivatives can be extracted directly from the output of the simulation and are given by
171 the central finite-difference derivative

$$173 \quad G_{np,q}(\mathbf{r}, \mathbf{s}) \approx \frac{G_{np}(\mathbf{r}, \mathbf{s} + \Delta q) - G_{np}(\mathbf{r}, \mathbf{s} - \Delta q)}{2\Delta q} \quad (2)$$

174
175 where $G_{np,q}(\mathbf{r}, \mathbf{s})$ is the spatial derivative of the Green's functions G_{np} around the source
176 position, \mathbf{s} is the source position, \mathbf{r} is the receiver position and Δq is the spatial grid
177 spacing. The Green's functions were calculated using a Gaussian source time function
178 with a frequency range of up to 5 Hz and a duration of 15 s. The recording positions for
179 the synthetic data map to the real locations of nine stations deployed on the volcano
180 during a seismic experiment carried out in February 2005, as shown in Figure 1. Since
181 Arenal is quite a dangerous environment (due to the frequent pyroclastic flows and the
182 ballistic bombardment of blocks and bombs), the stations were deployed on the flanks of
183 the volcano but, unfortunately, could not be placed close to the summit.

184

185 In the frequency domain, equation (1) can be written as:

186

$$187 \quad u_n(\mathbf{x}, \omega) = M_{pq}(\omega)G_{np,q}(\mathbf{x}, \omega) + G_{np}(\mathbf{x}, \omega)F_p(\omega) \quad (3)$$

188

189 where $u_n(\omega)$, $M_{pq}(\omega)$, $F_p(\omega)$, $G_{np}(\omega)$, $G_{np,q}(\omega)$, are the spectra of the displacements, of

190 the moment tensor components, of the single forces and of the components and of the

191 spatial derivatives of the Green's functions, respectively. The equation is solved

192 separately for each frequency. The results are then transformed into the time domain

193 using an inverse Fourier Transform. Equation (3) can be written in matrix form as:

194

$$195 \quad \mathbf{u} = \mathbf{Gm} \quad (4)$$

196

197 where \mathbf{u} is the data matrix, \mathbf{G} is matrix containing the Green's functions and derivatives,

198 \mathbf{m} is the moment tensor and single forces components' matrix. If N is the number of

199 seismograms used in the inversion, equation 4 can be also written in an explicit form as;

200

$$201 \quad \begin{bmatrix} u_1 \\ u_2 \\ \cdot \\ \cdot \\ \cdot \\ u_N \end{bmatrix} = \begin{bmatrix} g_{11,1} & g_{12,2} & g_{13,3} & g_{11,2} & g_{11,3} & g_{12,3} & g_{11} & g_{12} & g_{13} \\ g_{21,1} & g_{22,2} & g_{23,3} & g_{21,2} & g_{21,3} & g_{22,3} & g_{21} & g_{22} & g_{23} \\ g_{31,1} & g_{32,2} & g_{33,3} & g_{31,2} & g_{31,3} & g_{32,3} & g_{31} & g_{32} & g_{33} \\ \vdots & \vdots & \vdots & \vdots & \vdots & \vdots & \vdots & \vdots & \vdots \\ \vdots & \vdots & \vdots & \vdots & \vdots & \vdots & \vdots & \vdots & \vdots \\ g_{N1,1} & g_{N2,2} & g_{N3,3} & g_{N1,2} & g_{N1,3} & g_{N2,3} & g_{N1} & g_{N2} & g_{N3} \end{bmatrix} \cdot \begin{bmatrix} M_{11} \\ M_{22} \\ M_{33} \\ M_{12} \\ M_{13} \\ \vdots \\ M_{23} \\ F_1 \\ F_2 \\ F_3 \end{bmatrix} \quad (5)$$

202

203 with the assumption (due to the symmetry of the moment tensor) that

204

$$205 \quad \mathbf{g}_{np,q} = \begin{cases} \mathbf{G}_{np,q} & p = q \\ \mathbf{G}_{np,q} + \mathbf{G}_{nq,p} & p \neq q \end{cases} \quad n = 1,2,3,..N \quad (6)$$

206

207 The quality of our inversion procedure is tested through the evaluation of the misfit (\mathbf{R})

208 between calculated and observed data. \mathbf{R} can be expressed by the following equation:

209

$$210 \quad R = \frac{(\mathbf{u} - \mathbf{Gm})^T \mathbf{W}(\mathbf{u} - \mathbf{Gm})}{\mathbf{u}^T \mathbf{W} \mathbf{u}} \quad (7)$$

211

212 where \mathbf{W} is a diagonal weighting matrix of the quality of the waveforms. It can be

213 expressed in explicit matrix format as

214

$$215 \quad \mathbf{W} = \begin{bmatrix} w_1 & 0 & \cdots & 0 \\ 0 & w_2 & \cdots & 0 \\ \vdots & \vdots & \ddots & \vdots \\ 0 & 0 & \cdots & w_N \end{bmatrix} \quad (8)$$

216

217 The lowest value of the misfit \mathbf{R} indicates the best solution for \mathbf{m} . As equation 4 is a

218 linear equation, its least squares solution can be expressed as (Menke, 1984):

219

$$220 \quad \mathbf{m}^{\text{est}} = (\mathbf{G}^T \mathbf{W} \mathbf{G})^{-1} \mathbf{G}^T \mathbf{W} \mathbf{u} \quad (9)$$

221

222 where the superscript “T” denotes the transpose matrix and \mathbf{m}^{est} is the estimated moment-
223 tensor matrix. Since data recorded at different stations can show different noise
224 signatures, the weight matrix plays an important role in the inversion procedure.

225

226 **4. Description and results of Synthetic Tests**

227

228 The inversion technique is normally very sensitive to a range of effects present in
229 volcanic environments such as those associated with topography, near surface structures
230 and heterogeneities. To test the consistency and limitations of our inversion procedure we
231 performed a series of synthetic tests. In these tests we attempt to (i) investigate our ability
232 to retrieve the correct source time function and mechanism for a fixed source location
233 when random noise is added to our synthetic data, and (ii) analyze how a mislocated
234 source position can influence the inversion solution while highlighting the role played by
235 the single forces.

236

237 The use of synthetic tests is of crucial importance to contribute to the understanding of
238 the inversion technique and to retrieve the correct mechanism acting on the volcano.

239 Using 3D numerical simulations we generate synthetic signals with a Ricker wavelet
240 source time function with a central frequency of 2 Hz, shown in Figure 3. The source is
241 positioned under the crater summit where the real source is most likely to be located
242 (Benoit and McNutt, 1997; Hagerty et al., 2000; Mora et al., 2001; Lesage et al., 2006).

243 Source locations are not fully constrained at depth but the epicenters are probably located
244 in a small area centered under the active crater (Métaxian et al., 2002). We fix our source

245 point at a depth of 200 meters beneath the crater summit. The mechanism simulated is an
246 explosion ($M = 10^{12}$ Nm). No single forces are included. The inversion was performed
247 for both a moment tensor plus single forces (MT+SF), and moment tensor only (MT).

248

249 It is important to note that in the following tests the moment tensor parts of the source
250 solution are expressed in 10^{12} Nm, while the force parts are expressed in 10^9 N. This is
251 due to the fact that a force of 10^9 N will produce a displacement with the same amplitude
252 of a moment of 10^{12} Nm if their radiation patterns are ignored (radiation pattern can be
253 ignored because of the good azimuthal coverage of the deployment). We validate (not
254 shown here) that this holds for our station configuration, i.e. that the radiation patterns of
255 the obtained moments and forces do not introduce significant deviation from the general
256 rule outlined above. Consequently, if we plot moment and forces using the same scale,
257 forces will not be visible in the diagrams even if they contribute considerably to the total
258 amplitude of the signals.

259

260 The first test aims to show the ability of our inversion code to retrieve the exact
261 mechanism and source time function. Since we used the exact Green's functions
262 calculated for the exact source position, the correct solution is expected to be retrieved.
263 Figure 4 shows the results of the test for the moment tensor components plus single
264 forces (MT+SF) in the left panel and moment tensor only (MT) in the right panel using
265 the field location of the nine stations. Solutions are characterized by a small value of the
266 misfit (approximately equal to zero). Since the source time function and the mechanism
267 are perfectly recovered by the inversion, and the value of R is small, we can affirm that

268 the correct solution is retrieved by our inversion code for both solutions (MT and
269 MT+SF). Table 1 lists the values of the misfits of the inversions performed using
270 synthetic and real data.

271

272 Since data recorded on volcanoes can often have a low signal-to-noise ratio, we attempt
273 to simulate a real situation by adding noise to our synthetic data. In the frequency range
274 of interest, we contaminate our synthetic dataset with random noise derived from the
275 noise level of the real data recorded on Arenal. These data show a low level of
276 contamination of noise equally distributed at all the stations. The amplitude of the noise is
277 within 10% of the average rms amplitude (signal-to-noise ratio, SNR = 10). The
278 inversion is performed for the moment tensor components and the moment tensor
279 components plus single forces. Results of the test are illustrated in Figure 5. Spurious
280 single forces appear in the MT+SF inversion solution. Since the amplitude of the noise is
281 small, the solution is not dominated by the spurious forces and the source time function
282 and explosive mechanism are correctly recovered by both inversions (see M_{xx} , M_{yy} , M_{zz}
283 components for MT and MT+SF solution). In order to test how larger noise amplitudes
284 influence the solution we increased the noise level to 50% of the average rms amplitude,
285 which could be the case if strong tremor was recorded simultaneously with LP events.
286 The amplitude of the spurious forces increases with the increase in noise level. As shown
287 in Figure 6 (right panel) the MT solution remains stable and correct, while in the case of
288 MT+SF the spurious single forces strongly contaminate the solution. The source time
289 function and mechanism recovered along the diagonal components of the moment tensor
290 solution (MT+SF) are no longer correctly retrieved and the solutions do not look stable.

291 This leads to the conclusion that noise introduces a larger error into the inversion with
292 more free parameters.
293
294 Since spurious single forces can be generated when noisy data are used in the inversion,
295 we want to investigate how the presence of real single forces can influence the solution.
296 In order to understand the role played by single forces in the inversion procedure for both
297 MT and MT+SF solution, we perform synthetic tests in which different geometries are
298 simulated (e.g. pure volumetric source and a vertical crack with the normal parallel to the
299 x direction) along with including a strong single force in the west-east (x) direction.
300 Again twelve stations have been used along with a signal to noise ratio of 10. Results for
301 the pure volumetric source ($M = 10^{12}$ Nm) and single force ($F = 10^9$ N) are shown in
302 Figure 7. Solutions for the moment tensor components (Figure 7, right panel) are
303 correctly retrieved by the inversion procedure even though a real single force is included
304 in the actual input source. In the solution for the MT+SF (Figure 7, left panel), spurious
305 single forces are generated in the vertical and north-south directions, in addition to larger
306 amplitudes along the z direction. The amplitude of the west-east force is successfully
307 retrieved, while the source-time function exhibits “ringing” in the tail of the retrieved
308 signal. Results for a vertical crack with single west-east horizontal force are shown in
309 Figure 8. The MT inversion solution (Figure 8, right panel) is well resolved, but spurious
310 single forces are again generated for the MT+SF solution, left panel of Figure 8. For the
311 vertical crack the spurious force along the z direction has a slightly larger amplitude than
312 the one generated for a pure volumetric source. For both geometries along the off-
313 diagonal components, a small non-volumetric component is generated. The generation of

314 this component can be considered as an artifact of the inversion procedure and it does not
315 significantly affect the solution.

316

317 The same test has been performed using an input single force along the vertical direction.

318 The MT solutions are correct for pure volumetric sources and vertical crack geometries.

319 In the solution for MT+SF, the moment tensor part and the vertical force are again

320 correctly retrieved while spurious single forces are present in the north-south and west-

321 east directions. Since the same solutions have been obtained using a west-east and a

322 vertical input force, only solutions for the horizontal force is presented.

323

324 Finally a test is performed to analyze how the solution of the moment tensor inversion for

325 MT and MT+SF is influenced when an incorrect source position is used. The signal to

326 noise ratio is again 10. With this test we aim to resemble a realistic, and quite common,

327 situation in which the correct position of the seismic source is unknown and difficult to

328 determine. The mislocated source is fixed in a positioned 240 m in the x-direction, 345 m

329 in the y-direction and 500 m in the z-direction away from the correct source (located

330 under the crater summit at a depth of 200 m). In the test, an explosive source mechanism

331 has been simulated with no single forces included in the inversion. The solution is shown

332 in Figure 9. For the MT solution the explosive mechanism and the Ricker-like wavelet

333 source time function are well retrieved by the inversion. In the MT+SF solution spurious

334 single forces are generated, particularly in the z-direction. The amplitudes of the spurious

335 single forces originating from a mislocated source position are comparable to the

336 amplitudes of the forces generated when noise is added to our synthetic data (see Figure 5

337 and 9). This leads to the conclusion that in the presence of a noise with amplitude within
338 10% of the average rms, the solution is insensitive to the inaccurate location of the
339 source.

340

341 **5. Discussion of synthetic tests**

342

343 We performed the synthetic tests in order to constrain the inversion of the real data from
344 Arenal volcano. In particular, we wanted to investigate how different signal to noise
345 ratios, and errors in the source locations, influence the inversion solutions. We also tested
346 the inversion code using synthetic data generated with 3D numerical simulations. We
347 have shown that results for noisy data give stable MT solutions in which the source time
348 function and mechanism are correctly retrieved. In the case where forces are allowed in
349 the solutions (MT+SF), spurious single forces are generated with the largest amplitudes
350 in the z-direction. When the signal to noise ratio decreases, the amplitude of the spurious
351 single forces increases, strongly influencing the solution. When the signal to noise ratio is
352 decreased to 2, the source time function and mechanism are no longer retrieved in the
353 MT+SF solution. In addition, the spurious single forces entirely dominate the solution.
354 Finally, we tested the sensitivity of the inversion to source mislocation. In this case the
355 correct source time function and mechanism are correctly retrieved for the MT solution,
356 while solutions for the MT+SF give rise to spurious single forces. Since both the source
357 mislocation and noisy environment produced spurious single forces in MT+SF solution,
358 we investigated the possibility of neglecting the forces in our inversions, i.e. inverting for
359 the MT solution only, even if actual single forces are present in the source. We used two

360 mechanisms, a pure volumetric source and a vertical crack, both with a strong horizontal
361 single force (west-east direction). In both cases the solutions for the MT were correct. In
362 the MT+SF solutions, the moment tensor part and the true single force are correct, while
363 spurious single forces are generated on the other single force components. The same
364 results are obtained using a strong vertical input force.

365

366 From the obtained results we can affirm that spurious single forces are easily generated
367 under conditions common on volcanoes, such as noisy data and mislocated source
368 positions. Hence, particular care should be taken when interpreting the forces obtained
369 from the inversion of real data. On the contrary, for the station configuration in this study,
370 the MT solutions are always correct in the tests made, even if the actual single forces are
371 neglected in the inversion. This leads us to the conclusion that, in the presence of a well
372 constrained velocity model, MT solutions can be trusted even when noisy data are used in
373 the inversion and that real forces, if present, will not affect this solution. It is important to
374 note that the latter result is valid for Arenal volcano with this station distribution but
375 cannot be generalized for all volcanoes. Separate tests for each specific site and station
376 distribution should be performed. Performing these synthetic tests using the station
377 distribution from the 2005 seismic installation provides us with better understanding of
378 how different uncertainties in our data map onto the moment tensor solution. This will
379 allow us to reliably interpret the results from the inversion of the real data catalogue. An
380 example of an inversion of a single explosive event recorded in February 2005 is
381 presented in the following section.

382

383 **6. Application to real data**

384

385 During a seismic experiment, carried out from the 10th to the 21st of February 2005, nine
386 Güralp CMG40T seismometers, with mini-Titan recorders were deployed on Arenal
387 volcano. This temporary network recorded several events per day. From this database a
388 signal accompanying an explosion, occurring on the 14th of February at 21.40, was
389 selected for moment tensor inversion (Figure 10).

390

391 Métaxian et al. (2002) and Lesage et al. (2006) reported on signals recorded during
392 previous experiments carried out on Arenal in 1997. These signals, coming from the same
393 source region, have durations of only 7 s (e. g. path effects are not longer than 7 s), which
394 suggests that our 100 s long signals do not only represent path effects, but rather a
395 complicated source process or an amalgamation of several processes. This is apparent
396 from the spectrogram in Figure 10, where the onset of the signal has a broad spectrum
397 followed by the separated spectral lines. These lines could be interpreted as a harmonic
398 tremor triggered by an initial disturbance (Lesage et al., 2006). Although we consider our
399 velocity model as a reasonable approximation of the real structure, even small
400 uncertainties can prevent us from correctly inverting for such a long signal. This is
401 because uncertainties in the velocity model will primarily change the coda of the signal,
402 so in the case of a long source process this error accumulates with the time. For these
403 reasons, we will invert for the “trigger” part of the signal only. In order to analyze how,
404 and if, time-windowing of the signal influences our inversion we perform an additional
405 synthetic test. In this test we simulate an explosive mechanism (no single forces are

406 included) using synthetic signals generated by a 40 second long source time function. The
407 inversion is performed for the moment tensor components and moment tensor component
408 plus single forces for a source located 200 m under the crater summit. The duration of
409 both Green's functions and signals are reduced in the inversion code to 15 seconds and
410 tapered. Figure 11 shows the solutions for the MT+SF (left panel) and the MT (right
411 panel). In the solution for moment tensor components plus single forces, spurious single
412 forces are generated along the horizontal and vertical directions. The moment tensor
413 components for both solutions (with and without single forces allowed in the inversion)
414 are analyzed with the principal components analysis (Vasco, 1989). This analysis is based
415 on the singular value decomposition of the moment tensor components. Both solutions
416 are found to consist of 94% isotropic components. The amplitude of the source time
417 function is well retrieved by the inversion. This leads us to the conclusion that the
418 retrieval of the correct source mechanism is not influenced by reducing the length of the
419 signal and by using only the initial trace of the event.

420

421 To perform the inversion on the recorded event, after the deconvolution for instrument
422 responses, the data is converted from velocity to displacement measurements. The energy
423 peak is between 0.8 - 2 Hz, thus the signals are filtered within this band. The quality of
424 the inversion is again evaluated through the analysis of the misfit R. Solutions for
425 moment tensor components plus single forces, and moment tensor components only, are
426 analyzed. Nine stations have been utilized in the inversion. The location of the source is
427 constrained through the inversion procedure performing a grid search within the volume
428 of possible source points. The dimensions and location of the source volume were

429 restricted to possible locations identified in previous work carried out on Arenal (Hagerty
430 et al., 2000; Métaixian et al., 2002), according to which the source is likely to be located
431 in a small area with a radius of 0.3 km around the crater summit and at a depth of no
432 more than 600 meters. The values of the misfit are evaluated for accuracy of the solution;
433 the best is defined by the lowest misfit. Only misfits lower than 0.5 have been considered.
434 The low misfits are mostly concentrated in the north-west corner of our volume. Small
435 variations of the source position inside this volume do not alter the inversion results. This
436 was also seen with the source mislocation synthetic tests. Calculated and observed data
437 are compared in Figure 12 while the results of the inversion are shown in Figure 13.
438 Single forces, generated in east-west, north-south, and vertical direction appear in the
439 solution. F_z has a larger amplitude than F_x and F_y . Our synthetic tests demonstrated that
440 spurious single forces are easily generated with this station configuration. Therefore,
441 given the synthetic results, we cannot be sure if they are real or spurious. Furthermore,
442 we have shown that the solution for moment tensor components is relatively stable. For
443 these reasons we have concentrated on the solution for MT only, analyzing it using the
444 principal components analysis. The results give a strong isotropic component (87%) with
445 a small percentage of compensate linear vector dipoles (CLVD) (9%) and double couple
446 components (4%). Since our previous test showed spurious off-diagonal components, we
447 may not rely on the deviatoric part of the solution. These results lead us to the conclusion
448 that the mechanism generating this event is, as expected, an explosion. Assuming that the
449 shear modulus (μ) is 10 GPa, the estimated volume change (ΔV) associated with this
450 explosive event is 68 m^3 ($\Delta V = \mu M_o$ where M_o is the scalar seismic moment). The source
451 position was located at roughly 200 meters beneath the crater summit. Following the

452 approach of Jolly et al. (2010), we performed the inversion for different source depths;
453 the isotropic component percentage remains stable inside the source location volume with
454 a maximum value of 85%, but the relative percentage of CLVD and double couple
455 changes. Therefore, given the results from the synthetic tests, and considering that an
456 inversion of the explosive event produces an isotropic solution, we are confident that the
457 MT inversion can be applied to the data recorded during this deployment.

458

459 **7. Conclusions**

460

461 In this paper we present synthetic tests performed to examine how the errors involved in
462 the moment tensor inversion influence the correct retrieval of the source time function
463 and mechanism in the volcanic setting of Arenal volcano. In particular we focus our
464 attention on how the signal-to-noise-ratio, and a mislocated source position, influence the
465 results of the inversion performed for moment tensor components and moment tensor
466 components plus single forces. We show that spurious single forces are easily generated
467 when noisy data and mislocated source positions are included in the inversion. However,
468 we find that the inversion for MT only gives the correct MT components of the solution
469 even when the actual single forces are present in the source. This suggests that for this
470 volcano, and this station configuration, we should be careful in attaching physical
471 meaning to single forces. This information is used in the interpretation of the results of an
472 inversion for an explosive event recorded on Arenal in 2005. Analyzing the solution with
473 the principal components analysis of Vasco (1989), we are able to recover a
474 predominantly explosive mechanism for the analyzed event. Performing the inversion for

475 different source depth shows the stability of the isotropic component present in the
476 solution. This allows us to confidently invert for the different classes of data recorded on
477 Arenal in 2005 in order to retrieve and compare the source mechanisms generating a
478 range of observed events.

479

480 **Acknowledgements**

481

482 This work has been funded by Science Foundation Ireland (SFI). The authors wish to
483 acknowledge the Irish Centre for High-End Computing (ICHEC) for providing
484 computational facilities. We would also like to thank Dr Louis De Barros and Dr Shane
485 Tyrrell for useful comments on the manuscript. The fieldwork was partly supported by
486 the European Commission, 6th Framework Project – ‘VOLUME’, Contract No. 018471,
487 INSU-CNRS (ACI Risques naturels et changements climatiques), Université de Savoie
488 (BQR B2005-09), and projects n° 113-A6-503 and 113-A7-511 from Universidad de
489 Costa Rica and Instituto Costarricense de Electricidad. We thank the staff of Escuela
490 Centroamericana de Geología, Universidad de Costa Rica, and Instituto Costarricense de
491 Electricidad for their efficient logistical support. We would also like to thank P. Jousset
492 and an anonymous reviewer for detailed reviews which greatly improved the manuscript.

493

494 **References**

495

496 Aki, K. & Richards, P. G, 2002. Quantitative Seismology, 2nd ed., University
497 Science Books, Sausalito, California, 700 pp.

498

499 Alvarado, G., Barquero, R., 1997. Las señales sísmicas del volcán Arenal (Costa Rica) y
500 su relación con las fases eruptivas (1968–1986). *Ciencia e Tecnología*, 11 (1), 15–35.

501

502 Bean, C., Lokmer, I., O'Brien, G., 2008. The influence of near-surface on long-period
503 (LP) seismic signals and on moment tensor inversions: Simulated examples from Mt.
504 Etna. *Journal of Geophysical Research*, 113, B08308, doi:10.1029/2007JB005468.

505

506 Benoit, J.P. and McNutt, S.R., 1997. New constraints on source processes of volcanic
507 tremor at Arenal Volcano, Costa Rica, using broad-band seismic data. *Geophysical*
508 *Research Letters*, 24, 449-452.

509

510 Chouet, B. A., 1996. Long-period volcano seismicity: its source and use in eruption
511 forecasting. *Nature*, 380, 309-316.

512

513 Chouet, B. A., 2003. Volcano Seismology. *Pure and Applied Geophysics*, 160 (3), 739-
514 788.

515

516 Hagerty, M.T., Schwartz, S.Y., Garcés, M.A., Protti, M., 2000. Analysis of seismic and
517 acoustic observations at Arenal volcano, Costa Rica, 1995–1997. *Journal of Volcanology*
518 *and Geothermal researchResearch*, 101, 27-65.

519

520 Jolly, A., Sherburn, S., Jousset, P., and Kilgour, G., 2010. Eruption source processes

521 derived from seismic and acoustic observations of the 25 September 2007 Ruapehu
522 eruption North Island, New Zealand. *Journal of Volcanology and Geothermal Research*,
523 191, 33–45.

524

525 Jousset, P., Neuberg, J., and Jolly, A., 2004. Modelling low-frequency earthquakes in
526 a viscoelastic medium with topography. *Geophysical Journal International*, 159, 776–802.

527

528 Lesage, P., Mora, M.M, Alvarado, G., Pacheco, J., Métaxian, J. P., 2006. Complex
529 behavior and source model of the tremor at Arenal volcano, Costa Rica. *Journal of*
530 *Volcanology and Geothermal Research*, 157, 49–59.

531

532 Lokmer, I., Bean, C.J., Saccorotti, G., Patanè, D., 2007. Moment tensor inversion of LP
533 events recorded on Etna in 2004 using constraints obtained from wave simulation tests.
534 *Geophysical Research Letters*, 34, L22316, doi:10.1029/2007GL031902.

535

536 Lokmer, I., 2008. Long period seismic activity and moment tensor inversion in volcanic
537 environments: Application to Mount Etna. Unpublished Ph.D. Thesis, University College
538 Dublin, Ireland.

539

540 Lokmer, I., Saccorotti, G., Di Lieto, B., Bean, C. J., 2008. Temporal evolution of long-
541 period seismicity at Etna Volcano, Italy, and its relationships with the 2004-2005
542 eruption. *Earth and Planetary Science Letters*, 266, 205-220.

543

544 McNutt, S. R. (2005). Volcanic Seismology. Annual Review of Earth and Planetary
545 Sciences, 33 (1), 461-491, doi:10.1146/annurev.earth.33.092203.122459.

546

547 Menke, W., 1984. Geophysical data analysis: Discrete inverse theory. First edition,
548 Academic Press Inc., Orlando, Florida, 260 pp.

549

550 Métaxian, J.P., Lesage, P., Dorel, J., 1997. Permanent tremor of Masaya volcano,
551 Nicaragua: wavefield analysis and source location. Journal of Geophysical Research, 102,
552 22529– 22545.

553

554 Métaxian, J.P., Lesage, P., Valette, B., 2002. Locating sources of volcanic tremor and
555 emergent events by seismic triangulation: Application to Arenal volcano, Costa Rica.
556 Journal of Geophysical Research, 107, B10, 2243, doi:10.1029/2001JB000559.

557

558 Métaxian, J.P., O'Brien, G.S., Bean, C.J., Valette, B., Mora, M., 2009. Locating volcano-
559 seismic signals in the presence of rough topography: wave simulations on Arenal
560 volcano, Costa Rica. Geophysical Journal International, 179, 3, doi: 10.1111/j.1365-
561 246X.2009.04364.x

562

563 Mora, M.M, Lesage, P., Dorel, J., Bard, P., Metaxian, J.P., Alvarado G. E., Leandro C.,
564 2001. Study of seismic effects using H/V spectral ratios at Arenal Volcano, Costa Rica.
565 Geophysical Research Letters, 28, n.15, 2991-2994.

566

567 Mora, M.M., Lesage, P., Valette, B., Alvarado, G.E., Leandro, C., Metaxian, J. P., Dorel,
568 J., 2006. Shallow velocity structure and seismic site effects at Arenal volcano, Costa
569 Rica. *Journal of Volcanology and Geothermal Research*, 152, 121-139.
570

571 Neuberg, J. and Pointer, T., 2000. Effects of volcano-topography on seismic broadband
572 waveforms. *Geophysical Journal International*, 143, 239–248.
573

574 Neuberg, J., Luckett, R., Baptie, B., and Olsen, K., 2000. Models of tremor and low-
575 frequency earthquake swarms on Montserrat. *Journal of Volcanology and Geothermal*
576 *Research*, 101, 83–104.
577

578 O'Brien, G. S., Bean, C. J., 2004. A 3D discrete numerical elastic lattice method for
579 seismic wave propagation in heterogeneous media with topography. *Geophysical*
580 *Research Letters*, 31, L14608, doi:10.1029/2004GL020069.
581

582 Ohminato, T. and Chouet, B., 1997. A free-surface boundary condition for including
583 3D topography in the finite-difference method. *Bulletin of the Seismological Society of*
584 *America*, 87(2), 494–515
585

586 Ohminato, T., Chouet, B. A., Dawson, P., Kedar, S., 1998, Waveform inversion of very
587 long period impulsive signals associated with magmatic injection beneath Kilauea
588 Volcano, Hawaii. *Journal of Geophysical Research*, 103 (B10), 23839-23862
589

590 Soto, G.J., Alvarado, G.E., 2006. Eruptive history of Arenal Volcano, Costa Rica, 7 ka to
591 present. *Journal of Volcanology and Geothermal Research*, 157, 254-269.

592

593 Takei, Y. & Kumazawa, M., (1994). Why have the single force and torque been
594 excluded from seismic source models? *Geophysical Journal International*, 118 (1), 20-30.

595

596 Vasco, D. W., (1989). Deriving source-time functions using principal component
597 analysis, *Bulletin of the Seismological Society of America*, 79 (3), 711-730.

598

599 Williams-Jones, G., Stix, J., Heiligmann, M., Barquero, J., Fernandez, E., Gonzalez,
600 E.D., 2001. A model of degassing and seismicity at Arenal volcano, Costa Rica. *Journal*
601 *of Volcanology and Geothermal Research*, 108, 121–139.

602

603 **Figures captions**

604

605 Figure 1. Digital elevation model and station configuration used in our synthetic tests.
606 Arenal location is shown in the right-hand panel. The triangles represent the locations of
607 the stations deployed on Arenal during a seismic experiment carried out in 2005.

608

609 Figure 2. 1D velocity model used for Arenal. The blue and red lines indicate the P-wave
610 (V_p) and S-wave (V_s) velocities versus depth, respectively.

611

612 Figure 3. Ricker wavelet source time function (amplitude expressed in 10^{-12} Nm) used to
613 generate synthetic signals (top panel) and its spectrum (bottom panel).

614

615 Figure 4. Moment tensor component plus single forces solution (left panel) and moment
616 tensor components solution (right panel) for synthetic data generated with an explosive
617 mechanism and the Ricker wavelet source time function shown in Figure 4.

618

619 Figure 5. Moment tensor component plus single forces solution (left panel) and moment
620 tensor components solution (right panel) obtained when random noise is added to the
621 synthetic data (noise amplitude is equal to $1/10^{\text{th}}$ of the signal amplitude). Spurious single
622 forces are generated in the solution for moment tensor components plus single forces.

623 The correct solution should be: $F_x = 0$; $F_y = 0$; $F_z = 0$; $M_{xx} = 1$; $M_{yy} = 1$; $M_{zz} = 1$; $M_{xy} = 0$;
624 $M_{xz} = 0$; $M_{yz} = 0$.

625

626 Figure 6. Same as Figure 5, with noise amplitude equal to $1/2$ of the signal amplitude.

627 Spurious single forces are generated in the solution for moment tensor components plus
628 single forces, strongly affecting the MT+SF solution.

629

630 Figure 7. As Figure 5 (noise amplitude equal to $1/10^{\text{th}}$ of the signal amplitude). In this
631 case, a pure volumetric source geometry with a single force was simulated. The real force
632 is correctly retrieved while spurious single forces are generated in the other direction. The
633 correct solution should be: $F_x = 2$; $F_y = 0$; $F_z = 0$; $M_{xx} = 1$; $M_{yy} = 1$; $M_{zz} = 1$; $M_{xy} = 0$; $M_{xz} =$
634 0 ; $M_{yz} = 0$.

635

636 Figure 8. As Figure 5 (noise amplitude equal to $1/10^{\text{th}}$ of the signal amplitude) for a crack
637 plus single force source. The real force is correctly retrieved while spurious single forces
638 are generated in the other directions. The correct solution should be: $F_x = 2$; $F_y = 0$; $F_z = 0$;
639 $M_{xx} = 2$; $M_{yy} = 1$; $M_{zz} = 1$; $M_{xy} = 0$; $M_{xz} = 0$; $M_{yz} = 0$ (moment tensor inversion for vertical
640 crack with $\lambda = 2\mu$ where λ and μ are the Lamé parameters) .

641

642 Figure 9. Same as Figure 5 (noise amplitude equal to $1/10^{\text{th}}$ of the signal amplitude) for
643 an incorrect source position. The mislocated source position does not affect the solution
644 for moment tensor components. The correct time solution should be: $F_x = 0$; $F_y = 0$; $F_z =$
645 0 ; $M_{xx} = 1$; $M_{yy} = 1$; $M_{zz} = 1$; $M_{xy} = 0$; $M_{xz} = 0$; $M_{yz} = 0$.

646

647 Figure 10. Explosion recorded on 14th February, 2005 at 21.40. On the left, the original
648 waveform (top panel), spectrogram (middle panel) and filtered (0.8-2 Hz) waveform
649 (bottom panel) are shown. The black rectangle highlights the portion of the signal for
650 which we performed the moment tensor inversion.

651

652 Figure 11. Moment tensor component plus single forces solution (left panel) and moment
653 tensor components solution (right panel) obtained using a 40 second long source time
654 function (see text for details). The top right panel shows the original source time function
655 of 40 s. The black rectangle highlights the portion of the source used in the inversion.

656

657 Figure 12. Calculated (red line) and observed seismogram (blue line) are compared for
658 the waveform inversion of the explosion that occurred on the 14th February 2005 at 21.40
659 (amplitude expressed in 10^{-4} m).

660

661 Figure 13. Moment tensor component plus single forces solution (left panel) and moment
662 tensor components solution (right panel) obtained by waveform inversion of the
663 explosion that occurred on the 14th February 2005 at 21.40.

664

665 Table 1. The values of the misfit (R) obtained for the synthetic tests and for the inversion
666 of the explosive event that occurred on the 14th of February 2005, are listed for both
667 moment tensor components, solutions and moment tensor components plus single forces
668 solutions.

669

1 **Moment tensor inversion of Explosive Long Period events recorded on Arenal**
2 **Volcano, Costa Rica, constrained by synthetic tests.**

3

4 | R. Davi¹, G.S. O'Brien^{1,2}, I. Lokmer^{1,2}, C.J. Bean^{1,2}, P. Lesage³, [M.M. Mora](#).⁴

5

6

7 ¹Seismology and Computational Rock Physics Laboratory, School of Geological
8 Sciences, University College Dublin, Belfield, Dublin 4, Ireland.

9 ²Complex and Adaptive Systems Laboratory (CASL), University College Dublin,
10 Belfield, Dublin 4, Ireland.

11 ³Laboratoire de Géophysique Interne et Tectonophysique, CNRS, Université de Savoie,
12 73376 Le Bourget-du-Lac Cedex, France

13 | [⁴Escuela Centroamericana de Geología, Universidad de Costa Rica, Ciudad Universitaria](#)
14 [Rodrigo Facio, San Pedro de Montes de Oca, 214-2060 San José, Costa Rica.](#)

15

16 **Abstract**

17

18 In order to constrain the moment tensor solution of an explosive seismic event recorded
19 on Arenal volcano, Costa Rica, we perform tests using synthetic data. These data are
20 generated using a 3D model including the topography of the volcano and the best
21 estimation of the velocity model available for Arenal. Solutions for (i) the moment tensor
22 components, and (ii) the moment tensor plus single forces, are analysed. When noisy data
23 and mislocated sources are used in the inversion, spurious single forces are easily

24 generated in the solution for the moment tensor components plus single forces. Forces
25 also appear when the inversion is performed using an explosive event recorded on Arenal
26 in 2005. Synthetic tests indicate that these forces might be spurious. However the
27 mechanism is correctly retrieved by the inversion in both solutions. The ability to recover
28 the explosive mechanism for the 2005 event combined with the interpretative aids from
29 the synthetic tests will enable us to invert for the large variation in events observed on
30 Arenal.

31

32 Keywords: Arenal volcano, moment tensor inversion, single forces, synthetic tests

33

34 **1. Introduction**

35

36 Volcanoes are complex and challenging environments showing a great variety of
37 behaviour. A range of earthquake types are regularly recorded on volcanoes. They
38 include: high frequency tectonic-like events, ~~also known as volcano tectonic events,~~
39 (VT), explosions, long period events (LP) and tremor. VT events have energy in the
40 range of 2-20 Hz with very similar signatures to tectonic earthquakes. They are due to
41 brittle rock failure, generated by regional tectonic forces, dyke propagation or pore over-
42 pressure (McNutt, 2005). LP events and tremor are normally characterized by strongly
43 peaked spectra. Their energy is concentrated between 0.2 and 5 Hz and they are thought
44 to be caused by fluid movements inside volcanic conduits (Chouet, 2003). Since tremor
45 and LP events seem to have common characteristics, differing only in duration, some
46 authors believe they share the same source mechanism (Chouet, 1996; [Neuberg et al.](#),

47 | [2000](#)). These types of events often precede and accompany volcanic eruptions, hence a
48 | deeper knowledge of their source origin may be helpful in volcanic event forecasting.
49 | One of the most common tools used to retrieve the seismic source mechanism is a
50 | moment tensor inversion. The combination of moment tensor components represents a
51 | system of equivalent forces that produces the same wavefield as the actual physical
52 | processes at the source. Inverting for the seismic source mechanism has become a
53 | common procedure. Inversions for very long period events (VLP) have been successfully
54 | performed (Ohminato et al., 1998; Chouet et al., 2003) as the very long wavelengths are
55 | not influenced by structural heterogeneities. However, this is not always the case for
56 | inversions of LP events. The shortest wavelengths are sensitive to velocity structures and
57 | strong topographic effects (Bean et al., 2008; Lokmer et al., 2007; Lokmer [et al.](#), 2008;
58 | [Métaxian et al., 2009](#)). Such effects introduce many uncertainties in the inversion
59 | procedure that can lead to apparently stable, but erroneous solutions (Bean et al., 2008).
60 | In fact, due to the complexity of volcanic environments (e.g. the lack of sufficient
61 | structural information, the high degree of heterogeneity and the scattering effects due to
62 | the pronounced topography), it is quite difficult to recover a unique (and correct) source
63 | mechanism. The inclusion of single forces in the inversion procedure makes the recovery
64 | of the source mechanism an even more challenging task. However, single forces may be
65 | common in volcanic environments and have been modelled in other seismic source
66 | studies. Takei and [Kumarawa-Kumazawa](#) (1994) provide a theoretical justification for the
67 | physical existence of these forces. However, an accurate quantification of these forces is
68 | not available at present. This is due to the fact that an inversion procedure with an

69 increased numbers of free parameters is extremely sensitive to uncertainties in the near-
70 surface velocity model (Bean et al., 2008).

71
72 In this paper, we perform a moment tensor inversion of an explosive event recorded in
73 2005 on Arenal volcano, Costa Rica, using constraints obtained by synthetic tests.
74 Topographical and structural effects are reduced using the best estimation of velocity
75 model available for Arenal volcano and Green's functions are calculated including 15 m
76 resolution digital elevation model the real topography of the volcano. In the synthetic
77 tests we ~~constrain~~ assess our ability to retrieve the correct source time function and
78 mechanism when (i) random noise is added to the data, and (ii) the source location is not
79 accurately known. We also investigate how the presence of single forces affects the
80 moment tensor solution. We aim to quantify our ability to accurately recover the true
81 source from ~~a real seismic data world situation~~. The information obtained by performing
82 the synthetic tests is used in the analysis and interpretation of the solution of the inversion
83 performed on real explosion data from Arenal. The methodology used in the calculation
84 of the Green's functions, and in the inversion method, is provided herein. Results of our
85 synthetic tests, the inversion of the real event and the interpretation of the mechanism that
86 generates this event are also presented.

87

88 **2. Arenal volcano**

89

90 Arenal is a small strato-volcano located in north-western Costa Rica and is mainly
91 composed of tephra and lava flows (Soto and Alvarado, 2006); its location and

92 | [topography digital elevation model](#) are shown in Figure 1. It was [dormant for several](#)
93 | [centuries](#) until July 1968 when a [Peléan](#) eruption resulted in 78 fatalities and opened three
94 | new craters in the western flank. Arenal's explosive activity is still ongoing today and is
95 | preceded, and accompanied, by different types of seismic events. The most common
96 | types are LP events, explosions, spasmodic and harmonic tremor, rockfalls and sporadic
97 | volcano tectonic swarms (Alvarado [and Barquero et al.](#), 1997). Explosions and LP events
98 | have the same frequency range (1-3 Hz), but differ in amplitude. Explosions have larger
99 | amplitudes and are accompanied by a large, audible air-shock. The explosion coda often
100 | evolves into tremor (Hagerty et al., 2000). Tremor is the most common type of event at
101 | Arenal with a duration that can last for several hours and comprises spasmodic and
102 | harmonic. Harmonic tremor can be distinguished from spasmodic tremor by their
103 | regularly spaced frequency peaks with most of the energy concentrated between 0.9 and 2
104 | Hz. Spasmodic tremor energy spans 1-6 Hz. There is no clear difference in the genesis of
105 | spasmodic and harmonic tremor; the former can progressively evolve into the latter and
106 | vice-versa (Lesage et al., 2006). Most of the tremor exhibits a progressive gliding in
107 | frequency that can last tens to hundreds of seconds. The gliding phenomenon can be
108 | generated by pressure changes in the fluid inside the conduit (Hagerty et al., 2000). The
109 | number of seismic events can be variable during the day. However, in recent decades a
110 | decrease in the number and amplitude of explosions has been recognised (Lesage et al.,
111 | 2006). Arenal's seismicity is often accompanied by gas emissions produced during the
112 | explosions and by passive degassing in rhythmic pulses along the edge of the crater
113 | (William-Jones et al., 2001). The origin of these seismic events is, at present, not fully
114 | understood.

115

116 3. Methodology

117

118 The elastic Green's functions are defined as the Earth's response to an impulsive source
119 generated at a certain point (source location) and propagating to a receiver location in an
120 elastic Earth. The n^{th} -component of the displacement, recorded at position \mathbf{x} and time t ,
121 can be written as (Aki and Richards, 2002):

122

$$123 \quad u_n(\mathbf{x}, t) = M_{pq}(t) * G_{np,q}(\mathbf{x}, t) + F_p(t) * G_{np}(\mathbf{x}, t), \quad n, p, q = 1, 2, 3 \quad (1)$$

124

125 where M_{pq} is the force couple or dipole in the pq direction acting at the source, F_p is the
126 single force acting in the p direction, and G_{np} and $G_{np,q}$ represent the n^{th} components of
127 the corresponding medium responses (Green's functions) and their derivatives,
128 respectively. The asterisk indicates convolution and the summation convention applies.
129 Volcanoes are the most "promising" environments in which single forces are likely to be
130 found (Takei and Kumazawa, 1994), even if the existence of these single forces in the LP
131 process is, at present, not reliably constrained by experiments or observations. For VLP
132 events, Chouet (2003) attributes single forces to gravitational energy in the source
133 volume due to the ascent of a slug of gas in the volcanic conduit or by a volcanic jet
134 during an explosion. The latter phenomenon was also successfully modelled using single
135 forces in the recent work of Jolly et al. (2010). The reliability of the inversion results are
136 strongly dependent on the accuracy with which the Green's functions are calculated
137 (Lokmer, 2008). In the past, due to computational restrictions, Green's functions were

Field Code Changed

138 calculated only for a homogeneous half-space excluding topography. This approach leads
139 to misinterpretations because the seismic wavefield is sensitive to layered velocity
140 models and strongly affected by topographical scattering (Bean et al., 2008). However, in
141 the past decade, topography has been included in the calculation of Green's functions
142 (Ohimanto and Chouet, 2007; Neuber and Pointer, 2000; Jousset et al., 2004; Jolly et al.
143 2010). To avoid incorrect interpretations we require detailed information about the
144 medium i.e. a precise velocity model or near-accurate Green's functions relative to the
145 frequencies of interest. At present, detailed velocity models with structural information,
146 particularly related to the layers close to the surface, are extremely rare on volcanoes due
147 to the considerable cost and effort involved in producing such high resolution velocity
148 models. Therefore, synthetic tests provide a powerful tool for constraining the inversion
149 results and improving the reliability of such interpretations.

150

151 To calculate the Green's functions we use 3D-full wavefield numerical simulations
152 including topography and the "best" estimate of the velocity structure retrieved from
153 sounding using the spatial autocorrelation (SPAC) method, Métaxian et al., 1997, -and
154 seismic refraction experiments carried out on Arenal in 1997 (Mora et al., 2006). In this
155 study, we use the 3D Elastic Lattice Method (ELM), to simulate wave propagation in the
156 elastic medium (O'Brien and Bean, 2004). To calculate the Green's functions we use a 1-
157 D velocity model, see (Figure 2). This velocity model comprises two major layers
158 following the profile of the topography above a half space medium with velocities of 3.5
159 km/s for the P-waves (V_p) and 2.0 km/s for the S-waves (V_s) and a maximum density
160 equal to 2500 kg/m³. The numerical domain consists of a 13 x 11 x 6 km³ space where

161 topography is derived from the Digital Elevation Model (DEM) of the volcano using a
162 spatial grid step of 15 m. Long wavelengths are simulated using a model of large extent
163 of the model and with relatively small grid-step. Absorbing boundaries, 900 m thick, are
164 included in the model to avoid edge reflections and ensure the absorption of the longest
165 wavelengths. The top boundary of the model is a free surface including topography. To
166 calculate the Green's functions library for a large number of source locations within a
167 predefined source region, we adopt the Reciprocity Theorem (e.g. Aki and Richards,
168 2002). Green's functions are calculated over a volume (480 x 300 x 840 m³) of 4735
169 points located under the crater summit. In addition to calculating the Green's functions
170 for each single point source, we also required their spatial derivatives around the source
171 position. Spatial derivatives can be extracted directly from the output of the simulation
172 and are given by the central finite-difference derivative

$$174 \quad G_{np,q}(\mathbf{r}, \mathbf{s}) \approx \frac{G_{np}(\mathbf{r}, \mathbf{s} + \Delta\mathbf{q}) - G_{np}(\mathbf{r}, \mathbf{s} - \Delta\mathbf{q})}{2\Delta\mathbf{q}} \quad (2)$$

175
176 where $G_{np,q}(\mathbf{r}, \mathbf{s})$ is the spatial derivative of the Green's functions G_{np} around the source
177 position, \mathbf{s} is the source position, \mathbf{r} is the receiver position and $\Delta\mathbf{q}$ is the spatial grid
178 spacing. The Green's functions were calculated using a Gaussian source time function
179 with for a frequency range of up to 5 Hz and a duration of 15 s. The recording positions
180 for the synthetic data map to the real locations of nine stations deployed on the volcano
181 during a seismic experiment carried out in February 2005, as shown in Figure 31. Since
182 Arenal is quite a dangerous environment (due to the frequent pyroclastic flows and the

183 ballistic bombardment of blocks and bombs), the stations were deployed on the flanks of
184 the volcano but, unfortunately, could not be placed close to the summit.

185

186 | In the frequency domain ~~without the single forces term~~, equation (1) can be written as:

187

$$188 \quad u_n(\mathbf{x}, \omega) = M_{pq}(\omega)G_{np,q}(\mathbf{x}, \omega) + G_{np}(\mathbf{x}, \omega)F_p(\omega) \quad (3)$$

189

190 | where $u_n(\omega)$, $M_{pq}(\omega)$, $F_p(\omega)$, $G_{np}(\omega)$, $G_{np,q}(\omega)$ are the spectra of the displacements, of
191 the moment tensor components, ~~of the single forces and~~ of the components and of
192 the spatial derivatives of the Green's functions, respectively. The equation is solved

193 separately for each frequency. The results are then transformed into the time domain

194 using an inverse Fourier Transform. Equation (3) can be written in matrix form as:

195

$$196 \quad \mathbf{u} = \mathbf{Gm} \quad (4)$$

197

198 where \mathbf{u} is the data matrix, \mathbf{G} is matrix containing the Green's functions and derivatives,

199 | \mathbf{m} is the moment tensor and single forces components' matrix. If N is the number of

200 seismograms used in the inversion, equation 4 can be also written in an explicit form as;

201

$$\begin{matrix}
202 \\
\end{matrix}
\begin{bmatrix} u_1 \\ u_2 \\ \cdot \\ \cdot \\ u_N \end{bmatrix} = \begin{bmatrix} g_{11,1} & g_{12,2} & g_{13,3} & g_{11,2} & g_{11,3} & g_{12,3} & g_{11} & g_{12} & g_{13} \\ g_{21,1} & g_{22,2} & g_{23,3} & g_{21,2} & g_{21,3} & g_{22,3} & g_{21} & g_{22} & g_{23} \\ g_{31,1} & g_{32,2} & g_{33,3} & g_{31,2} & g_{31,3} & g_{32,3} & g_{31} & g_{32} & g_{33} \\ \vdots & \vdots & \vdots & \vdots & \vdots & \vdots & \vdots & \vdots & \vdots \\ \vdots & \vdots & \vdots & \vdots & \vdots & \vdots & \vdots & \vdots & \vdots \\ g_{N1,1} & g_{N2,2} & g_{N3,3} & g_{N1,2} & g_{N1,3} & g_{N2,3} & g_{N1} & g_{N2} & g_{N3} \end{bmatrix} \begin{bmatrix} M_{11} \\ M_{22} \\ M_{33} \\ M_{12} \\ M_{13} \\ M_{23} \\ F_1 \\ F_2 \\ F_3 \end{bmatrix} \quad (5)$$

203

204 with the assumption (due to the symmetry of the moment tensor) that

205

$$\begin{matrix}
206 \\
\end{matrix}
g_{np,q} = \begin{cases} G_{np,q} & p = q \\ G_{np,q} + G_{nq,p} & p \neq q \end{cases} \quad n = 1,2,3,..N \quad (6)$$

207

208 The quality of our inversion procedure is tested through the evaluation of the misfit (R)

209 between calculated and observed data. R can be expressed by the following equation:

210

$$\begin{matrix}
211 \\
\end{matrix}
R = \frac{(\mathbf{u} - \mathbf{Gm})^T \mathbf{W}(\mathbf{u} - \mathbf{Gm})}{\mathbf{u}^T \mathbf{W} \mathbf{u}} \quad (7)$$

212

213 where \mathbf{W} is a diagonal weighting matrix of the quality of the waveforms. It can be

214 expressed in explicit matrix format as

215

216
$$W = \begin{bmatrix} w_1 & 0 & \cdots & 0 \\ 0 & w_2 & \cdots & 0 \\ \vdots & \vdots & \ddots & \vdots \\ 0 & 0 & \cdots & w_N \end{bmatrix} \quad (8)$$

217

218 The lowest value of the misfit R indicates the best solution for \mathbf{m} . As equation 4 is a
 219 linear equation, its least squares solution can be expressed as (Menke, 1984):

220

221
$$\mathbf{m}^{\text{est}} = (\mathbf{G}^T \mathbf{W} \mathbf{G})^{-1} \mathbf{G}^T \mathbf{W} \mathbf{u} \quad (9)$$

222

223 where the superscript “T” denotes the transpose matrix and \mathbf{m}^{est} is the estimated moment-
 224 tensor matrix. Since data recorded at different stations can show different noise

225 signatures, the weight matrix plays an important role in the inversion procedure. ~~A small~~
 226 ~~amount of noise in the data can results in large errors in the derivation of source~~
 227 ~~mechanisms, even leading to erroneous solutions. A good example of how noise can~~
 228 ~~influence the retrieval of the correct solution is given by Aster et al. (2005, pp. 73-79).~~

229

230

231 **4. Description and results of Synthetic Tests**

232

233 The inversion technique is normally very sensitive to a range of effects present in
 234 volcanic environments such as those associated with topography, near surface structures
 235 and heterogeneities. To test the consistency and limitations of our inversion procedure we
 236 performed a series of synthetic tests. In these tests we attempt to (i) investigate our ability

237 to retrieve the correct source time function and mechanism for a fixed source location
238 when random noise is added to our synthetic data, and (ii) analyze how a mislocated
239 source position can influence the inversion solution while highlighting the role played by
240 the single forces.

241

242 | The use of synthetic tests is of crucial importance ~~for to contribute to the full~~
243 | understanding of the inversion technique and to retrieve the correct mechanism acting on
244 | the volcano. Using 3D numerical simulations we generate synthetic signals with a Ricker
245 | wavelet source time function with a central frequency of 2 Hz, shown in Figure 43. The
246 | source is positioned under the crater summit where the real source is most likely to be
247 | located (Benoit and McNutt, 1997; Hagerty et al., 2000; Mora et al., 2001; Lesage et al.,
248 | 2006). Source locations are not fully constrained at depth but the epicenters are probably
249 | located in a small area centered under the active crater (Métaxian et al., 2002). We fix our
250 | source point at a depth of 200 meters beneath the crater summit. The mechanism
251 | simulated is an explosion ($M = 10^{12}$ Nm). No single forces are included. The inversion
252 | was performed for both a moment tensor plus single forces (MT+SF), and moment tensor
253 | only (MT).

254

255 | It is important to note that in the following tests the moment tensor parts of the source
256 | solution are expressed in 10^{12} Nm, while the force parts are expressed in 10^9 N. This is
257 | due to the fact that a force of 10^9 N will produce ~~the same~~ displacement with the same
258 | amplitude of a moment of 10^{12} Nm if their radiation patterns are ignored (radiation
259 | pattern ~~this can be done-ignored due to because of~~ the good azimuthal coverage of the

260 deployment). We validate (not shown here) that this holds for our station configuration,
261 i.e. that the radiation patterns of the obtained moments and forces do not introduce
262 significant deviation from the ~~relationship-general rule~~ outlined above. Consequently, if
263 we plot moment and forces using the same scale, forces will not be visible in the
264 diagrams even if they ~~considerably~~ contributes considerably to the total amplitude of the
265 signals.
266

267 The first test aims to show the ability of our inversion code to retrieve the exact
268 mechanism and source time function. Since we used the exact Green's functions
269 calculated for the exact source position, the correct solution is expected to be retrieved.
270 Figure ~~5-4~~ shows the results of the test for the moment tensor components plus single
271 forces (MT+SF) in the left panel and moment tensor only (MT) in the right panel using
272 the field location of the nine stations. Solutions are characterized by a small value of the
273 misfit (approximately equal to zero). Since the source time function and the mechanism
274 are perfectly recovered by the inversion, and the value of R is small, we can affirm that
275 the correct solution is retrieved by our inversion code for both solutions (MT and
276 MT+SF). Table 1 lists the values of the misfits of the inversions performed using
277 synthetic and real data.
278

279 Since data recorded on volcanoes can often have a low signal-to-noise ratio, we attempt
280 to simulate a real situation by adding noise to our synthetic data. In the frequency range
281 of interest, we contaminate our synthetic dataset with random noise derived from the
282 noise level of the real data recorded on Arenal. These data show a low level of

283 contamination of noise equally distributed at all the stations. The amplitude of the noise is
284 within 10% of the average rms amplitude (signal-to-noise ratio, SNR = 10). The
285 inversion is performed for the moment tensor components and the moment tensor
286 components plus single forces. Results of the test are illustrated in Figure 65. Spurious
287 single forces appear in the MT+SF inversion solution. Since the amplitude of the noise is
288 small, the solution is not dominated by the spurious forces and the source time function
289 and explosive mechanism are correctly recovered by both inversions (see M_{xx} , M_{yy} ,
290 M_{zz} diagonal components for MT and MT+SF solution). In order to test how larger noise
291 amplitudes influence the solution we increased the noise level to 50% of the average rms
292 amplitude, which could be the case if strong tremor was recorded simultaneously with LP
293 events. The amplitude of the spurious forces increases with the increase in noise level. As
294 shown in Figure 76 (right panel) the MT solution remains stable and correct, while in the
295 case of MT+SF the spurious single forces strongly ~~influences~~ ~~contaminates~~ the solution.
296 The source time function and mechanism recovered along the diagonal components of the
297 moment tensor solution (MT+SF) are no longer correctly retrieved and the solutions do
298 not look stable. This leads to the conclusion that noise introduces a larger error into the
299 inversion with more free parameters.

300

301 Since spurious single forces can be generated when noisy data are used in the inversion,
302 we want to investigate how the presence of real single forces can influence the solution.
303 In order to understand the role played by single forces in the inversion procedure for both
304 MT and MT+SF solution, we perform synthetic tests in which different geometries are
305 simulated (e.g. pure volumetric source and a vertical crack with the normal parallel to the

306 | x direction) along with including a strong single force in the Westwest-East-east (x)
307 | direction. Again twelve stations have been used along with a signal to noise ratio of 10.
308 | Results for the pure volumetric source ($M = 10^{12}$ Nm) and single force ($F = 10^9$ N) are
309 | shown in Figure 87. Solutions for the moment tensor components (Figure 87, right panel)
310 | are correctly retrieved by the inversion procedure even though a real single force is
311 | included in the actual input source. In the solution for the MT+SF (Figure 87, left panel),
312 | spurious single forces are generated in the vertical and Northnorth-South-south directions,
313 | in addition to larger amplitudes along the z direction. The amplitude of the Westwest-
314 | East-east force is successfully retrieved, while the source-time function exhibits “ringing”
315 | in the tail of the retrieved signal. Results for a vertical crack with single Westwest-East
316 | east horizontal force are shown in Figure 98. The MT inversion solution (Figure 98, right
317 | panel) is well resolved, but spurious single forces are again generated for the MT+SF
318 | solution, left panel of Figure 98. For the vertical crack the spurious force along the z
319 | direction has a slightly larger amplitude than the one generated for a pure volumetric
320 | source. For both geometries along the off-diagonal components, a small non-volumetric
321 | component is generated. The generation of this component can be considered as an
322 | artifact of the inversion procedure and it does not significantly affect the solution.
323 |
324 | The same test has been performed using an input single force along the vertical direction.
325 | The MT solutions are correct for pure volumetric sources and vertical crack geometries.
326 | In the solution for MT+SF, the moment tensor part and the vertical force are again
327 | correctly retrieved while spurious single forces are present in the Northnorth-South-south
328 | and Westwest-East-east directions. Since the same solutions have been obtained using a

329 ~~Westwest-East east~~ and a vertical input force, only solutions for the horizontal force is
330 presented.

331

332 Finally a test is performed to analyze how the solution of the moment tensor inversion for
333 MT and MT+SF is influenced when an incorrect source position is used. The signal to
334 noise ratio is again 10. With this test we aim to resemble a realistic, and quite common,
335 situation in which the correct position of the seismic source is unknown and difficult to
336 determine. The mislocated source is fixed in a positioned 240 m in the x-direction, 345 m
337 in the y-direction and 500 m in the z-direction away from the correct source (located
338 under the crater summit at a depth of 200 m). In the test, an explosive source mechanism
339 has been simulated with no single forces included in the inversion. The solution is shown
340 in Figure ~~409~~. For the MT solution the explosive mechanism and the Ricker-like wavelet
341 source time function are well retrieved by the inversion. In the MT+SF solution spurious
342 single forces are generated, particularly in the z-direction. The amplitudes of the spurious
343 single forces originating from a mislocated source position are comparable to the
344 amplitudes of the forces generated when noise is added to our synthetic data (see Figure ~~6~~
345 ~~5~~ and ~~409~~). This leads to the conclusion that in the presence of a noise with amplitude
346 within 10% of the average rms, the solution is insensitive to the ~~precise-inaccurate~~
347 location of the source.

348

349 **5. Discussion of synthetic tests**

350

351 We performed the synthetic tests in order to constrain the inversion of the real data from
352 Arenal volcano. In particular, we wanted to investigate how different signal to noise
353 ratios, and ~~wrong errors in the source~~ locations ~~of the source~~, influence the inversion
354 solutions. We also tested the inversion code using synthetic data generated with 3D
355 numerical simulations. We have shown that results for noisy data give stable MT
356 solutions in which the source time function and mechanism are correctly retrieved. In the
357 case where forces are allowed in the solutions (MT+SF), spurious single forces are
358 generated with the largest amplitudes in the z-direction. When the signal to noise ratio
359 decreases, the amplitude of the spurious single forces increases, strongly influencing the
360 solution. When the signal to noise ratio is decreased to 2, the source time function and
361 mechanism are no longer retrieved in the MT+SF solution. In addition, the spurious
362 single forces entirely dominate the solution. Finally, we tested the sensitivity of the
363 inversion to source mislocation. In this case the correct source time function and
364 mechanism are correctly retrieved for the MT solution, while solutions for the MT+SF
365 give rise to spurious single forces. Since both the source mislocation and noisy
366 environment produced spurious single forces in MT+SF solution, we investigated the
367 possibility of neglecting the forces in our inversions, i.e. inverting for the MT solution
368 only, even if actual single forces are present in the source. We used two mechanisms, a
369 pure volumetric source and a vertical crack, both with a strong horizontal single force
370 (~~Westwest-East-east~~ direction). In both cases the solutions for the MT were correct. In the
371 MT+SF solutions, the moment tensor part and the true single force are correct, while
372 spurious single forces are generated on the other single force components. The same
373 results are obtained using a strong vertical input force.

374

375 From the obtained results we can affirm that spurious single forces are easily generated
376 under conditions common on volcanoes, such as noisy data and mislocated source
377 positions. Hence, particular care should be taken when interpreting the forces obtained
378 from the inversion of real data. On the contrary, for the station configuration in this study,
379 the MT solutions are always correct in the tests made, even if the actual single forces are
380 neglected in the inversion. This leads us to the conclusion that, in the presence of a well
381 constrained velocity model, MT solutions can be trusted even when noisy data are used in
382 the inversion and that real forces, if present, will not affect this solution. It is important to
383 note that the latter result is valid for Arenal volcano with this station distribution but
384 cannot be generalized for all volcanoes. Separate tests for each specific site and station
385 distribution should be performed. Performing these synthetic tests using the station
386 distribution from the 2005 seismic installation provides us with better understanding of
387 how different uncertainties in our data map onto the moment tensor solution. This will
388 allow us to reliably interpret the results from the inversion of the real data catalogue. An
389 example of an inversion of a single explosive event recorded in February 2005 is
390 presented in the following section.

391

392 **6. Application to real data**

393

394 During a seismic experiment, carried out from the 10th to the 21st of February 2005, nine
395 Guralp CMG40T seismometers, with mini-Titan recorders were deployed on Arenal
396 volcano. This temporary network recorded several events per day. From this database a

397 signal accompanying an explosion, occurring on the 14th of February at 21.40, was
398 selected for moment tensor inversion (Figure [44-10](#)).
399

400 Métaixian et al. (2002) and Lesage et al. (2006) reported on signals recorded during
401 previous experiments carried out on Arenal in 1997. These signals, coming from the same
402 source region, have durations of only 7 s ([e. g. path effects are not longer than 7 s](#)), which
403 suggests that our 100 s long signals do not only represent path effects, but rather a
404 complicated source process or an amalgamation of several processes. This is apparent
405 from the spectrogram in Figure [44-10](#), where the onset of the signal has a broad spectrum
406 followed by the separated spectral lines. These lines could be interpreted as a harmonic
407 tremor triggered by an initial disturbance (Lesage et al., 2006). Although we consider our
408 velocity model as a reasonable approximation of the real structure, even small
409 uncertainties can prevent us from correctly inverting for such a long signal. This is
410 because uncertainties in the velocity model will primarily change the coda of the signal,
411 so in the case of a long source process this error accumulates with the time. For these
412 reasons, we will invert for the “trigger” part of the signal only. In order to analyze how,
413 and if, ~~the~~ time-windowing of the signal influences our inversion we perform an
414 additional synthetic test. In this test we simulate an explosive mechanism (no single
415 forces are included) using synthetic signals generated by a 40 second long source time
416 function. The inversion is performed for the moment tensor components and moment
417 tensor component plus single forces [for a source located 200 m under the crater summit](#).
418 The duration of both Green’s functions and signals are reduced in the inversion code to
419 15 seconds and tapered. Figure [42-11](#) shows the solutions for the MT+SF (left panel) and

420 the MT (right panel). In the solution for moment tensor components plus single forces,
421 spurious single forces are generated along the horizontal and vertical directions. The
422 moment tensor components for both solutions (with and without single forces allowed in
423 the inversion) are analyzed with the principal components analysis (Vasco, 1989). This
424 analysis is based on the singular value decomposition of the moment tensor components.
425 Both solutions are found to consist of 94% isotropic components. The amplitude of the
426 source time function is well retrieved by the inversion. This leads us to the conclusion
427 that the retrieval of the correct source mechanism is not influenced by reducing the length
428 of the signal and by using only the initial trace of the event.

429

430 To perform the inversion on the recorded event, after the deconvolution for instrument
431 responses, the data is converted from velocity to displacement measurements. The energy
432 peak is between 0.8 - 2 Hz, thus the signals are filtered within this band. The quality of
433 the inversion is again evaluated through the analysis of the misfit R . Solutions for
434 moment tensor components plus single forces, and moment tensor components only, are
435 analyzed. Nine stations have been utilized in the inversion. The location of the source is
436 constrained through the inversion procedure performing a grid search within the volume
437 of possible source points. The dimensions and location of the source volume were
438 restricted to possible locations identified in previous work carried out on Arenal (Hagerty
439 et al., 2000; Métaxian et al., 2002), according to which the source is likely to be located
440 in a small area with a radius of 0.3 km around the crater summit and at a depth of no
441 more than 600 meters. The values of the misfit are evaluated for accuracy of the solution;
442 the best is defined by the lowest misfit. Only misfits lower than 0.5 have been considered.

443 | The low misfits are mostly concentrated in the ~~Northnorth-Westwest~~ corner of our
444 | volume. Small variations of the source position inside this volume do not alter the
445 | inversion results. This was also seen with the source mislocation synthetic tests.

446 | Calculated and observed data are compared in ~~Figure 13-12~~ while the results of the
447 | inversion are shown in Figure ~~1413~~. Single forces, generated in ~~Easteast-Westwest~~,
448 | ~~Northnorth-Southsouth~~, and vertical direction appear in the solution. F_z has a larger
449 | amplitude than F_x and F_y . Our synthetic tests demonstrated that spurious single forces are
450 | easily generated with this station configuration. Therefore, given the synthetic results, we
451 | cannot be sure if they are real or spurious. Furthermore, we have shown that the solution
452 | for moment tensor components is relatively stable. For these reasons we have
453 | concentrated on the solution for MT only, analyzing it using the principal components
454 | analysis. The results give a strong isotropic component (87%) with a small percentage of
455 | compensate linear vector dipoles (CLVD) (9%) and double couple components (4%).
456 | Since our previous test showed spurious off-diagonal components, we may not rely on
457 | the deviatoric part of the solution. These results lead us to the conclusion that the
458 | mechanism generating this event is, as expected, an explosion. Assuming that the shear
459 | modulus (μ) is 10 GPa, the estimated volume change (ΔV) associated with this explosive
460 | event is 68 m^3 ($\Delta V = \mu M_0$ where M_0 is the scalar seismic moment). The source position
461 | was located at roughly 200 meters beneath the crater summit. Following the approach of
462 | Jolly et al. (2010), we performed the inversion for different source depths; ~~The~~ isotropic
463 | component percentage remains stable inside the source location volume with a maximum
464 | value of 85%, but the relative percentage of CLVD and double couple changes.

465 | Therefore, given the results from the synthetic tests, and considering that an inversion of

466 the explosive event produces an isotropic solution, we are confident that the MT
467 inversion can be applied to the ~~LP~~ data recorded during this deployment.

468

469 7. Conclusions

470

471 In this paper we present synthetic tests performed to examine how the errors involved in
472 the moment tensor inversion influence the correct retrieval of the source time function
473 and mechanism in the volcanic setting of Arenal volcano. In particular we focus our
474 attention on how the signal-to-noise-ratio, and a mislocated source position, influence the
475 results of the inversion performed for moment tensor components and moment tensor
476 components plus single forces. We show that spurious single forces are easily generated
477 when noisy data and mislocated source positions are included in the inversion. ~~On the~~
478 ~~contrary~~ However, we find that the inversion for MT only gives the correct MT
479 components of the solution even when the actual single forces are present in the source.
480 This suggests that for this volcano, and this station configuration, we should be careful in
481 attaching physical meaning to single forces. This information is used in the interpretation
482 of the results of an inversion for an explosive event recorded on Arenal in 2005.

483 Analyzing the solution with the principal components analysis of Vasco (1989), we are
484 able to recover a predominantly explosive mechanism for the analyzed event. Performing
485 the inversion for different source depth shows the stability of the isotropic component
486 present in the solution. This allows us to ~~confidentially-confidently~~ invert for the ~~other~~,
487 different classes of data recorded on Arenal in 2005 in order to retrieve and compare the
488 source mechanisms generating a range of observed events.

489

490 **Acknowledgements**

491

492 This work has been funded by Science Foundation Ireland (SFI). The authors wish to
493 acknowledge the Irish Centre for High-End Computing (ICHEC) for providing
494 computational facilities. We would also like to thank Dr Louis De Barros and Dr Shane
495 Tyrrell for useful comments on the manuscript. The fieldwork was partly supported by
496 the European Commission, 6th Framework Project – ‘VOLUME’, Contract No. 018471,
497 INSU-CNRS (ACI Risques naturels et changements climatiques), Université de Savoie
498 (BQR B2005-09), and projects n° 113-A6-503 and 113-A7-511 from Universidad de
499 Costa Rica and Instituto Costarricense de Electricidad. We thank the staff of Escuela
500 Centroamericana de Geología, Universidad de Costa Rica, and Instituto Costarricense de
501 Electricidad for their efficient logistical support. [We would also like to thank P. Jousset
502 and an anonymous reviewer for detailed reviews which greatly improved the manuscript.](#)

503

504 **References**

505

506 Aki, K. & Richards, P. G, 2002. Quantitative Seismology, 2nd ed., University
507 Science Books, Sausalito, California, 700 pp.

508

509 ~~Aster, R. C., Borchers, B., Thurber, C. H., 2005. Parameter Estimation and Inverse
510 Problems. Elsevier Academic Press, 300 pp.~~

511

512 Alvarado, G., Barquero, R., 1997. Las señales sísmicas del volcán Arenal (Costa Rica) y
513 su relación con las fases eruptivas (1968–1986). [Ciencia e- Tecnología](#), 11 (1), 15–35.
514

515 Bean, C., Lokmer, I., O’Brien, G., 2008. The influence of near-surface on long-period
516 (LP) seismic signals and on moment tensor inversions: Simulated examples from Mt.
517 Etna. *Journal of Geophysical Research*, 113, B08308, doi:10.1029/2007JB005468.
518

519 Benoit, J.P. and McNutt, S.R., 1997. New constraints on source processes of volcanic
520 tremor at Arenal Volcano, Costa Rica, using broad-band seismic data. *Geophysical*
521 *Research Letters*, 24, 449-452.
522

523 Chouet, B. A., 1996. Long-period volcano seismicity: its source and use in eruption
524 forecasting. *Nature*, 380, 309-316.
525

526 Chouet, B. A., 2003. Volcano Seismology. *Pure and Applied Geophysics*, 160 (3), 739-
527 788.
528

529 Hagerty, M.T., Schwartz, S.Y., Garcés, M.A., Protti, M., 2000. Analysis of seismic and
530 acoustic observations at Arenal volcano, Costa Rica, 1995–1997. *Journal of Volcanology*
531 *and Geothermal Research*, 101, 27-65.
532

533 [Jolly, A., Sherburn, S., Jousset, P., and Kilgour, G., 2010. Eruption source processes](#)
534 [derived from seismic and acoustic observations of the 25 September 2007 Ruapehu](#)

535 [eruption North Island, New Zealand. Journal of Volcanology and Geothermal Research,](#)
536 [191, 33–45.](#)

537

538 [Jousset, P., Neuberg, J., and Jolly, A., 2004. Modelling low-frequency earthquakes in](#)
539 [a viscoelastic medium with topography. Geophysical Journal International, 159, 776–802.](#)

540

541 [Lesage, P., Mora, M.M., Alvarado, G., Pacheco, J., Métaixian, J. P., 2006. Complex](#)
542 [behavior and source model of the tremor at Arenal volcano, Costa Rica. Journal of](#)
543 [Volcanology and Geothermal Research, 157, 49–59.](#)

544

545

546 Lokmer, I., Bean, C.J., Saccorotti, G., Patanè, D., 2007. Moment tensor inversion of LP
547 events recorded on Etna in 2004 using constraints obtained from wave simulation tests.
548 Geophysical Research Letters, 34, L22316, doi:10.1029/2007GL031902.

549

550 Lokmer, I., 2008. Long period seismic activity and moment tensor inversion in volcanic
551 environments: Application to Mount Etna. Unpublished Ph.D. Thesis, University College
552 Dublin, Ireland.

553

554 Lokmer, I., Saccorotti, G., Di Lieto, B., Bean, C. J., 2008. Temporal evolution of long-
555 period seismicity at Etna Volcano, Italy, and its relationships with the 2004-2005
556 eruption. [Earth and Planetary Science Letters](#), 266, 205-220.

557

558 | McNutt, S. R. (2005). Volcanic Seismology. Annual- Review- of Earth and Planetary-
559 | Sci-ences, 33 (1), 461-491, doi:10.1146/annurev.earth.33.092203.122459.

560

561 | Menke, W., 1984. Geophysical data analysis: Discrete inverse theory. First edition,
562 | Academic Press Inc., Orlando, Florida, 260 pp.

563

564 | Métaxian, J.P., Lesage, P., Dorel, J., 1997. Permanent tremor of Masaya volcano,
565 | Nicaragua: wavefield analysis and source location. Journal of Geophysical Research, 102,
566 | 22529– 22545.

567

568 | Métaxian, J.P., Lesage, P., Valette, B., 2002. Locating sources of volcanic tremor and
569 | emergent events by seismic triangulation: Application to Arenal volcano, Costa Rica.
570 | Journal of Geophysical Research, 107, B10, 2243, doi:10.1029/2001JB000559.

571

572 | Métaxian, J.P., O'Brien, G.S., Bean, C.J., Valette, B., Mora, M., 2009. Locating volcano-
573 | seismic signals in the presence of rough topography: wave simulations on Arenal
574 | volcano, Costa Rica. Geophysical Journal International, 179, 3, doi: 10.1111/j.1365-
575 | 246X.2009.04364.x

576

577 | Mora, M.M, Lesage, P., Dorel, J., Bard, P., Metaxian, J.P., Alvarado G. E., Leandro C.,
578 | 2001. Study of seismic effects using H/V spectral ratios at Arenal Volcano, Costa Rica.
579 | Geophysical Research Letters, 28, n.15, 2991-2994.

580

581 Mora, M.M., Lesage, P., Valette, B., Alvarado, G.E., Leandro, C., Metaxian, J. P., Dorel,
582 J., 2006. Shallow velocity structure and seismic site effects at Arenal volcano, Costa
583 Rica. *Journal of Volcanology and Geothermal Research*, 152, 121-139.

584

585 [Neuberg, J. and Pointer, T., 2000. Effects of volcano-topography on seismic broadband](#)
586 [waveforms. *Geophysical Journal International*, 143, 239–248.](#)

587

588 [Neuberg, J., Luckett, R., Baptie, B., and Olsen, K., 2000. Models of tremor and low-](#)
589 [frequency earthquake swarms on Montserrat. *Journal of Volcanology and Geothermal*](#)
590 [*Research*, 101, 83–104.](#)

591

592 O'Brien, G. S., Bean, C. J., 2004. A 3D discrete numerical elastic lattice method for
593 seismic wave propagation in heterogeneous media with topography. *Geophysical*
594 *Research Letters*, 31, L14608, doi:10.1029/2004GL020069.

595

596 [Ohminato, T. and Chouet, B., 1997. A free-surface boundary condition for including](#)
597 [3D topography in the finite-difference method. *Bulletin of the Seismological Society of*](#)
598 [*America*, 87\(2\), 494–515](#)

599

600 Ohminato, T., Chouet, B. A., Dawson, P., Kedar, S., 1998, Waveform inversion of very
601 long period impulsive signals associated with magmatic injection beneath Kilauea
602 Volcano, Hawaii. *Journal of Geophysical Research*, 103 (B10), 23839-23862

603

Formatted: Don't adjust space between Asian text and numbers

604 | Soto, G.J., Alvarado, G.E., 2006. Eruptive history of Arenal Volcano, Costa Rica, 7 ka to
605 | present. Journal of Volcanology and Geothermal Research, 157, 254-269.

606

607 | Takei, Y. & Kumazawa, M., (1994). Why have the single force and torque been
608 | excluded from seismic source models? Geophysical Journal International, 118 (1), 20-
609 | 30.

610

611 | Vasco, D. W., (1989). Deriving source-time functions using principal component
612 | analysis, Bulletin of the Seismological Society of America, 79 (3), 711-730.

613

614 | Williams-Jones, G., Stix, J., Heiligmann, M., Barquero, J., Fernandez, E., Gonzalez,
615 | E.D., 2001. A model of degassing and seismicity at Arenal volcano, Costa Rica. Journal
616 | of Volcanology and Geothermal Research, 108, 121–139.

617

618 | **Figures captions**

619

620 | Figure 1. ~~Arenal location map and topography.~~ Digital elevation model and station
621 | configuration used in our synthetic tests. Arenal location is shown in the right-hand
622 | panel. The triangles represent the locations of the stations deployed on Arenal during a
623 | seismic experiment carried out in 2005.

624

625 | Figure 2. 1D velocity model used for Arenal. The blue and red lines indicate the P-wave
626 | (V_p) and S-wave (V_s) velocities versus depth, respectively.

627

628 | ~~Figure 3. used in our synthetic tests. The stars represent the locations of the stations~~
629 ~~deployed on Arenal during a seismic experiment carried out in 2005.~~

630

631 | Figure 43. Ricker wavelet source time function (amplitude expressed in 10^{-12} Nm) used to
632 generate synthetic signals (top panel) and its spectrum (bottom panel).

633

634 | Figure 54. Moment tensor component plus single forces solution (left panel) and moment
635 tensor components solution (right panel) for synthetic data generated with an explosive
636 mechanism and the Ricker wavelet source time function shown in Figure 4.

637

638 | Figure 65. Moment tensor component plus single forces solution (left panel) and moment
639 tensor components solution (right panel) obtained when random noise is added to the
640 synthetic data (noise amplitude is equal to $1/10^{\text{th}}$ of the signal amplitude). Spurious single
641 forces are generated in the solution for moment tensor components plus single forces.

642 The correct solution should be: $F_x = 0$; $F_y = 0$; $F_z = 0$; $M_{xx} = 1$; $M_{yy} = 1$; $M_{zz} = 1$; $M_{xy} = 0$;

643 $M_{xz} = 0$; $M_{yz} = 0$.

644

645 | Figure 76. Same as Figure 65, with noise amplitude equal to $1/2$ of the signal amplitude.

646 Spurious single forces are generated in the solution for moment tensor components plus
647 single forces, strongly affecting the MT+SF solution.

648

649 | Figure 87. As Figure 6-5 (noise amplitude equal to $1/10^{\text{th}}$ of the signal amplitude). In this
650 | case, a pure volumetric source geometry with a single force was simulated. The real force
651 | is correctly retrieved while spurious single forces are generated in the other direction. The
652 | correct solution should be: $F_x = 2$; $F_y = 0$; $F_z = 0$; $M_{xx} = 1$; $M_{yy} = 1$; $M_{zz} = 1$; $M_{xy} = 0$; $M_{xz} =$
653 | 0 ; $M_{yz} = 0$.

654

655 | Figure 98. As Figure 6-5 (noise amplitude equal to $1/10^{\text{th}}$ of the signal amplitude) for a
656 | crack plus single force source. The real force is correctly retrieved while spurious single
657 | forces are generated in the other directions. The correct solution should be: $F_x = 2$; $F_y = 0$;
658 | $F_z = 0$; $M_{xx} = 2$; $M_{yy} = 1$; $M_{zz} = 1$; $M_{xy} = 0$; $M_{xz} = 0$; $M_{yz} = 0$ (moment tensor inversion for
659 | vertical crack with $\lambda = 2\mu$ where λ and μ are the Lamé parameters) .

660

661 | Figure 109. Same as Figure 6-5 (noise amplitude equal to $1/10^{\text{th}}$ of the signal amplitude)
662 | for an incorrect source position. The mislocated source position does not affect the
663 | solution for moment tensor components. The correct time solution should be: $F_x = 0$; $F_y =$
664 | 0 ; $F_z = 0$; $M_{xx} = 1$; $M_{yy} = 1$; $M_{zz} = 1$; $M_{xy} = 0$; $M_{xz} = 0$; $M_{yz} = 0$.

665

666 | Figure 110. Explosion recorded on 14th February, 2005 at 21.40. On the left, the original
667 | waveform (top panel), spectrogram (middle panel) and filtered (0.8-2 Hz) waveform
668 | (bottom panel) are shown. The black rectangle highlights the portion of the signal for
669 | which we performed the moment tensor inversion.

670

671 | Figure ~~42~~11. Moment tensor component plus single forces solution (left panel) and
672 | moment tensor components solution (right panel) obtained using a 40 second long source
673 | time function (see text for details). The top right panel shows the original source time
674 | function of 40 s. The black rectangle highlights the portion of the source used in the
675 | inversion.

676

677 | Figure ~~43~~12. Calculated (red line) and observed seismogram (blue line) are compared for
678 | the waveform inversion of the explosion that occurred on the 14th February 2005 at 21.40
679 | (amplitude expressed in 10^{-4} m).

680

681 | Figure ~~44~~13. Moment tensor component plus single forces solution (left panel) and
682 | moment tensor components solution (right panel) obtained by waveform inversion of the
683 | explosion that occurred on the 14th February 2005 at 21.40.

684

685 | Table 1. The values of the misfit (R) obtained for the synthetic tests and for the inversion
686 | of the explosive event that occurred on the 14th of February 2005, are listed for [both](#)
687 | moment tensor components ~~only~~ [solutions](#) and moment tensor components plus single
688 | forces [solutions](#).

689

Figure 1
[Click here to download high resolution image](#)

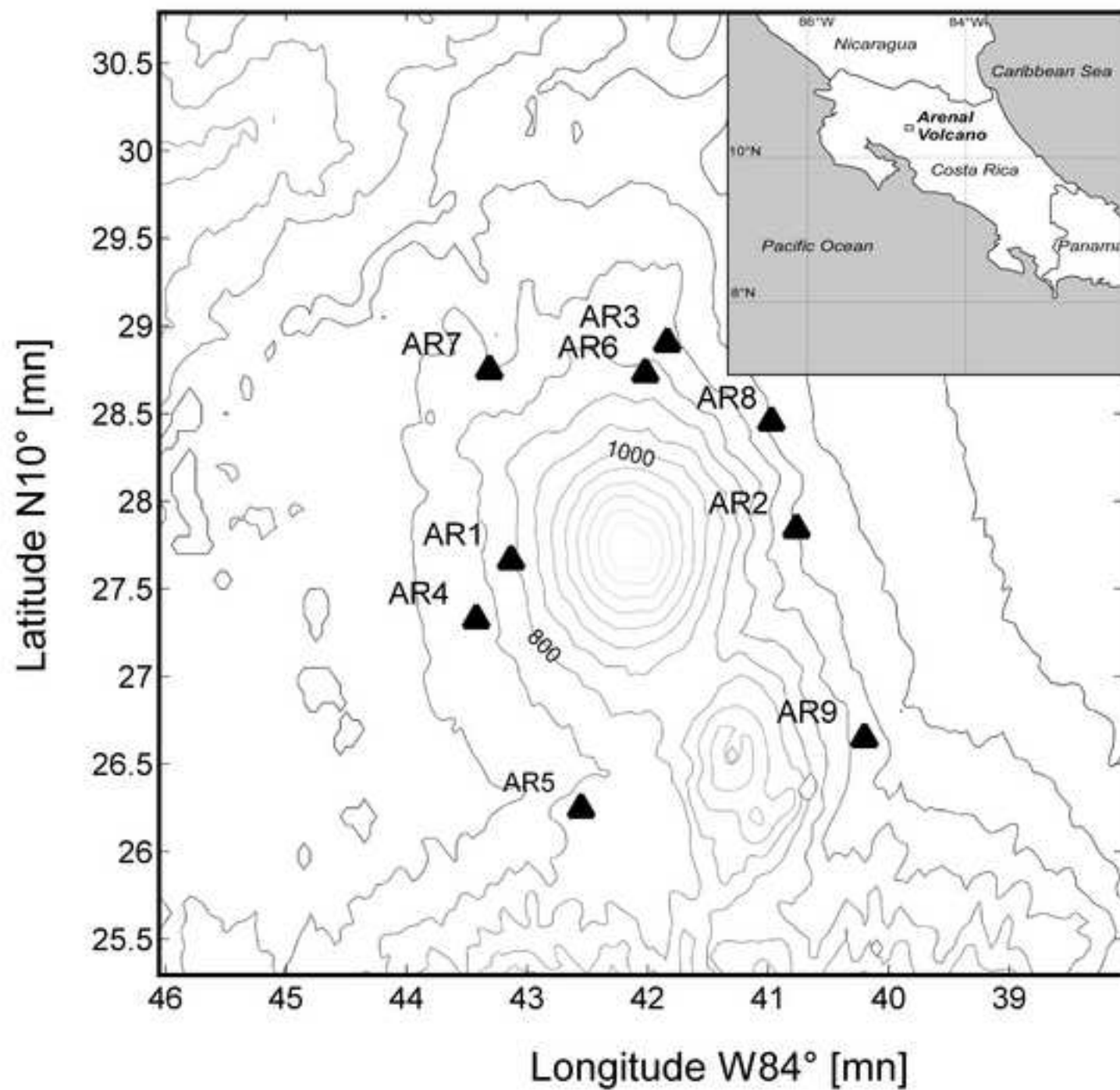


Figure 2
[Click here to download high resolution image](#)

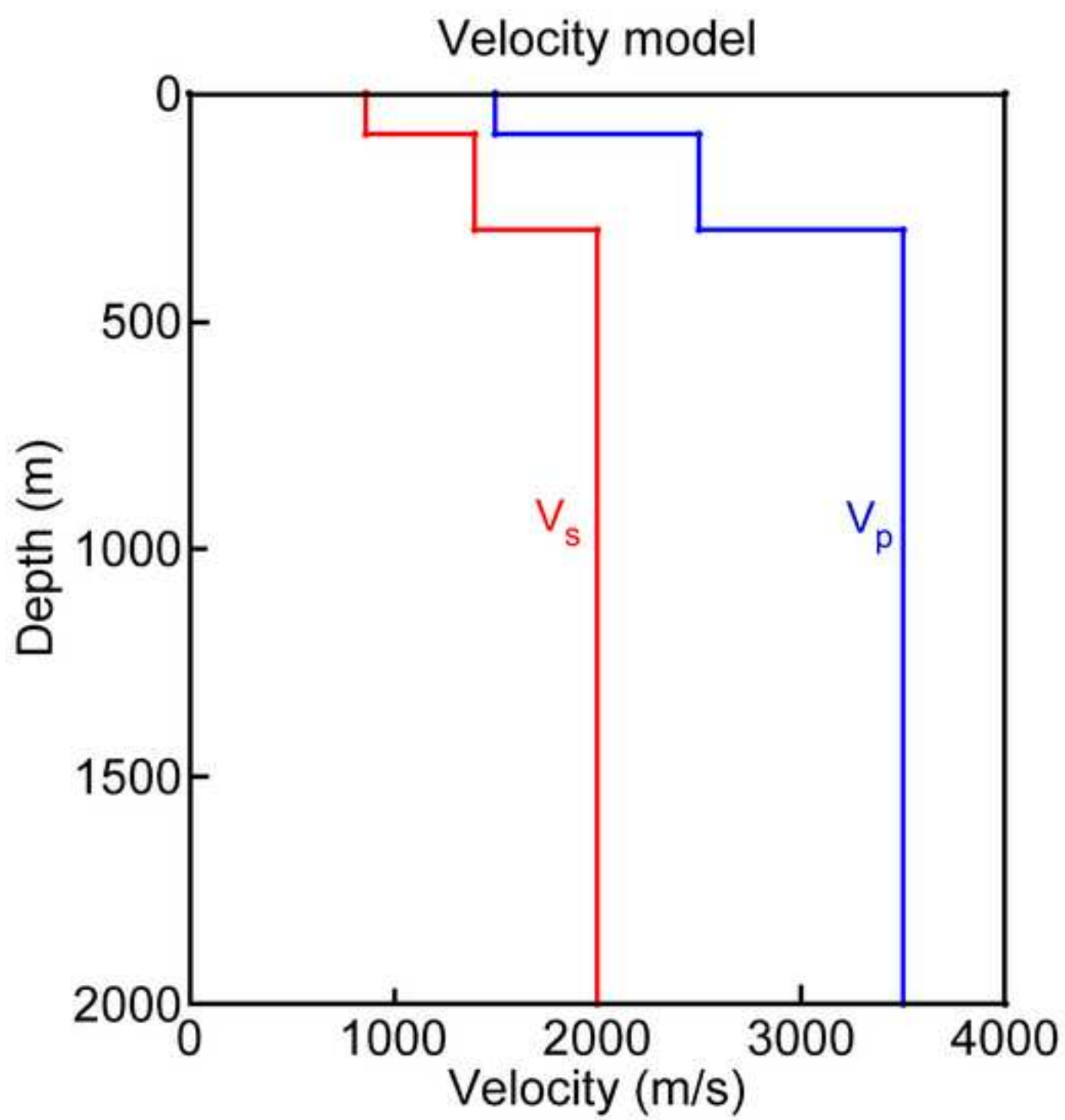


Figure 3
[Click here to download high resolution image](#)

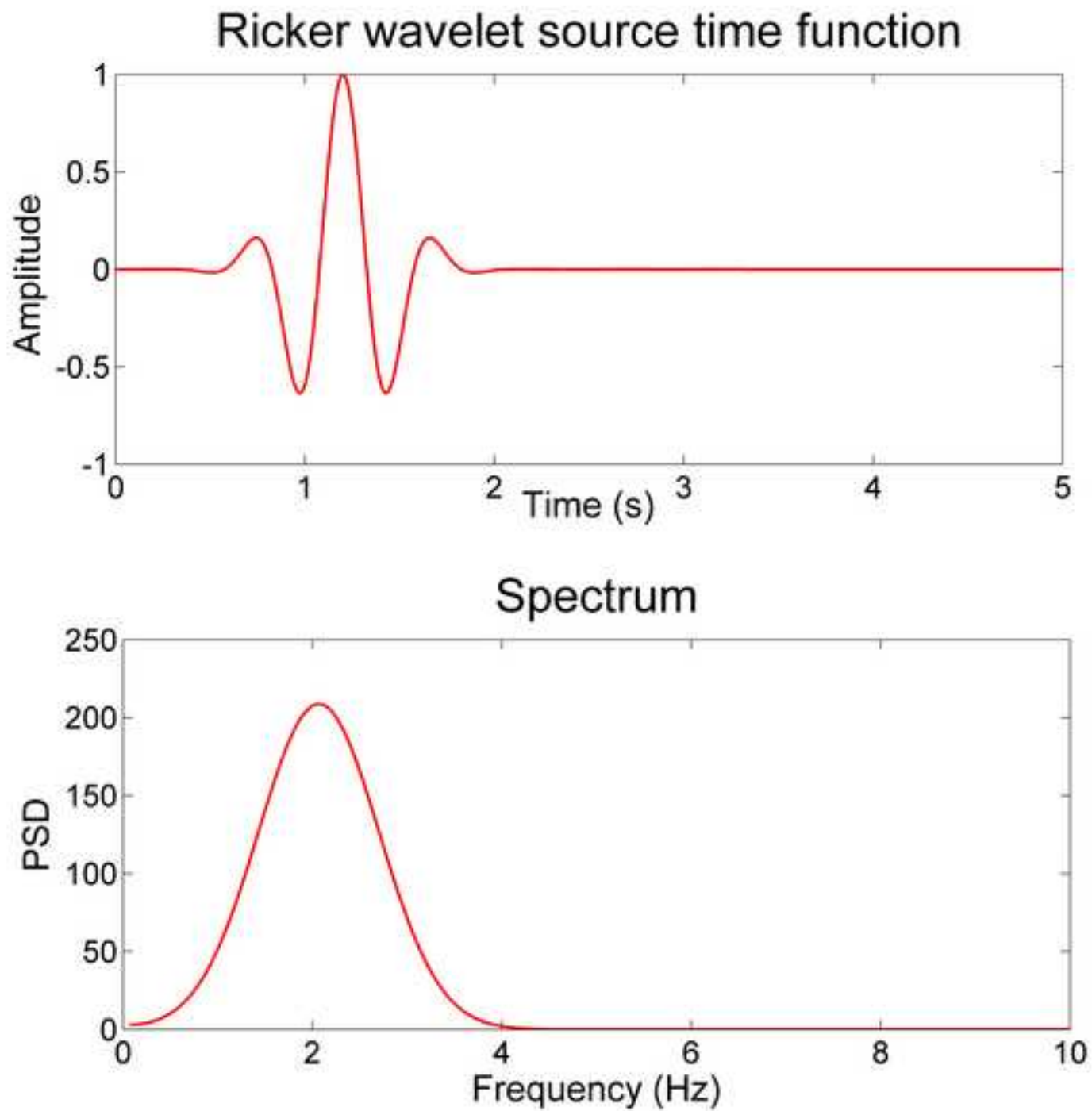
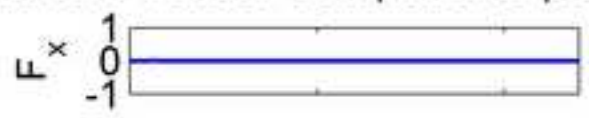


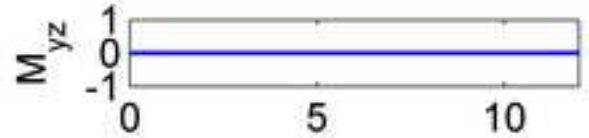
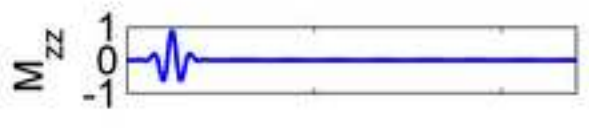
Figure 4

[Click here to download high resolution image](#)

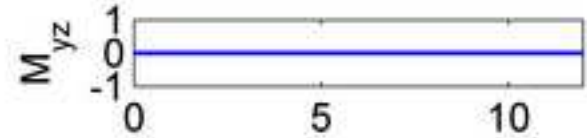
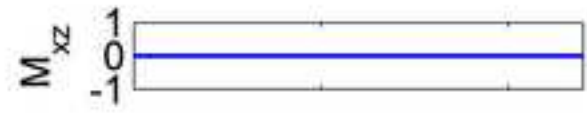
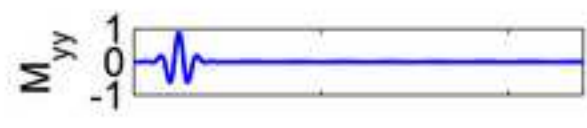
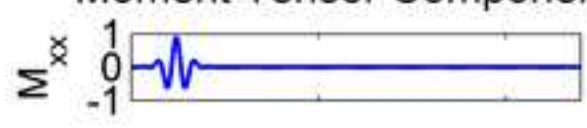
Moment Tensor Components plus Single Forces



$[F]=10^9 \text{ N}$
 $[M]=10^{12} \text{ Nm}$



Moment Tensor Components



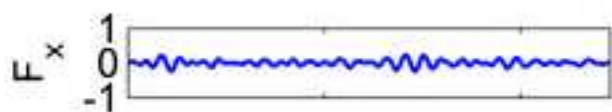
Time [s]

Time [s]

Figure 5

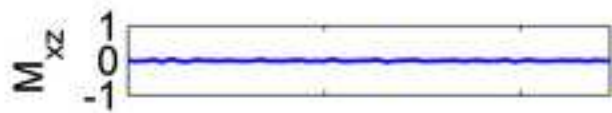
[Click here to download high resolution image](#)

Moment Tensor Components plus Single Forces



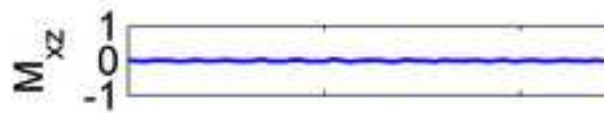
$$[F]=10^9 \text{ N}$$

$$[M]=10^{12} \text{ Nm}$$



Time [s]

Moment Tensor Components



Time [s]

Figure 6

[Click here to download high resolution image](#)

Moment Tensor Components plus Single Forces

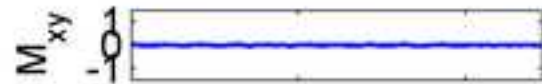


$[F]=10^9$ N
 $[M]=10^{12}$ Nm



Time [s]

Moment Tensor Components

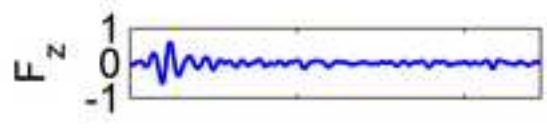


Time [s]

Figure 7

[Click here to download high resolution image](#)

Moment Tensor Components plus Single Forces



$[F]=10^9 \text{ N}$
 $[M]=10^{12} \text{ Nm}$

Moment Tensor Components



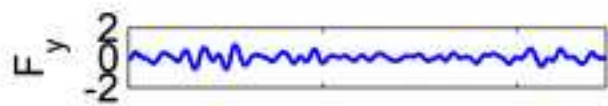
Time [s]

Time [s]

Figure 8

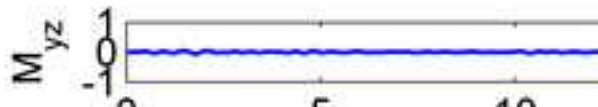
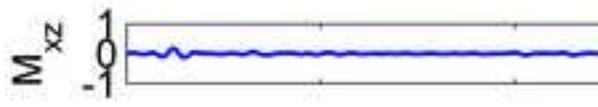
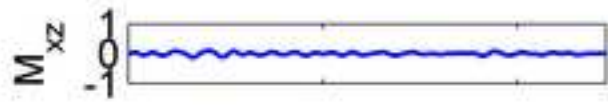
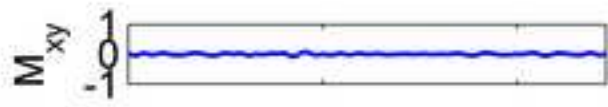
[Click here to download high resolution image](#)

Moment Tensor Components plus Single Forces



$[F]=10^9$ N
 $[M]=10^{12}$ Nm

Moment Tensor Components



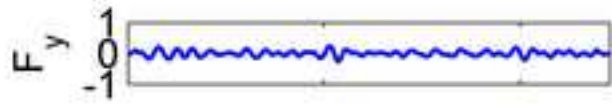
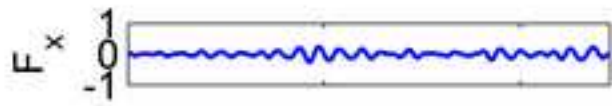
Time [s]

Time [s]

Figure 9

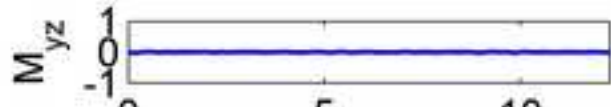
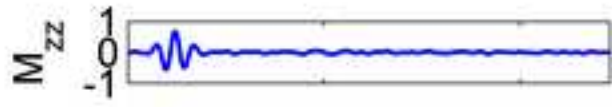
[Click here to download high resolution image](#)

Moment Tensor Components plus Single Forces



$[F]=10^9 \text{ N}$
 $[M]=10^{12} \text{ Nm}$

Moment Tensor Components



Time [s]

Time [s]

Figure 10
[Click here to download high resolution image](#)

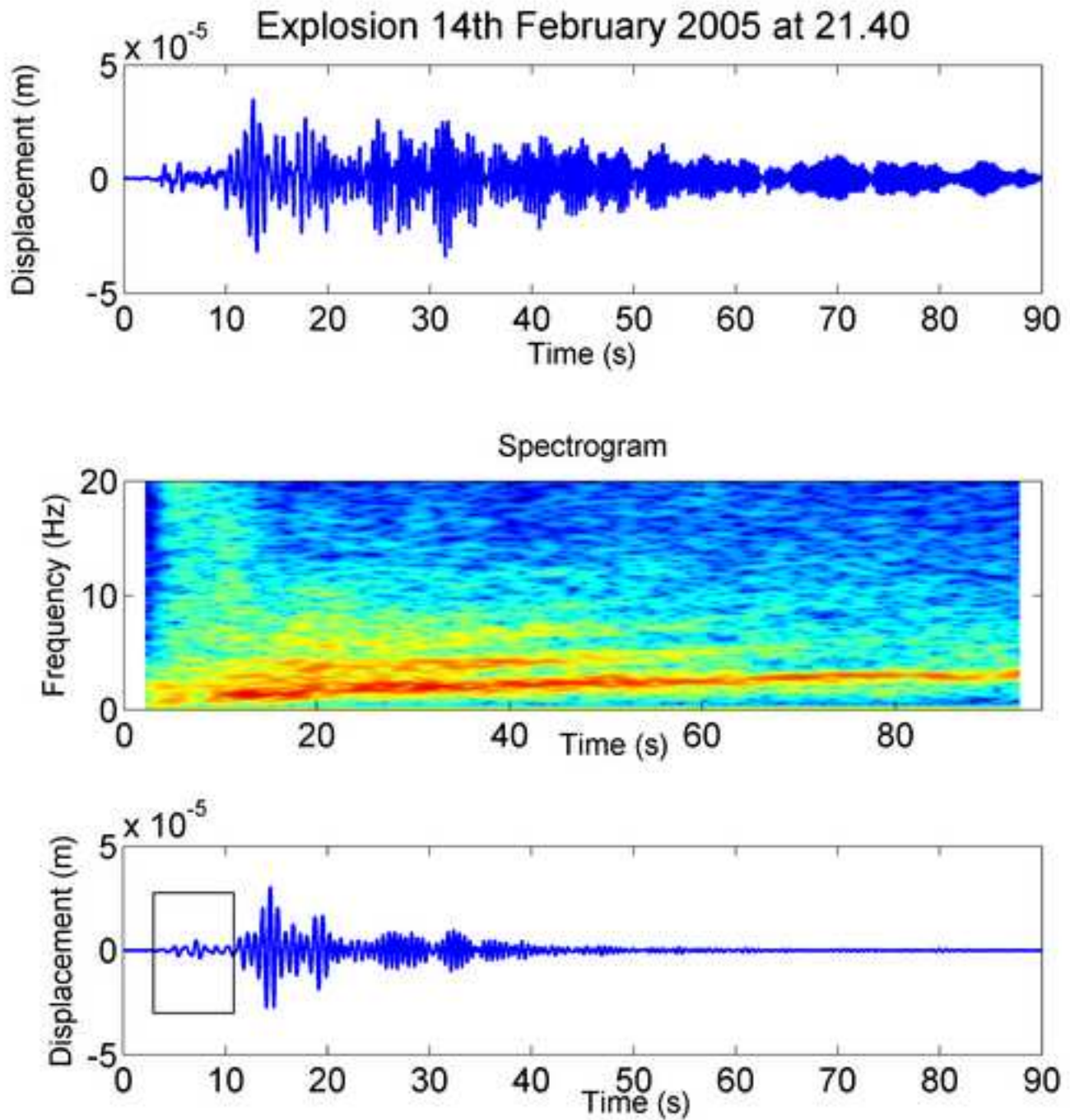
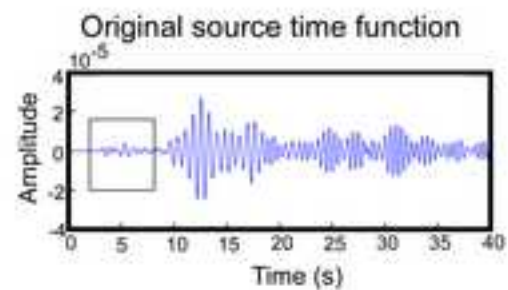
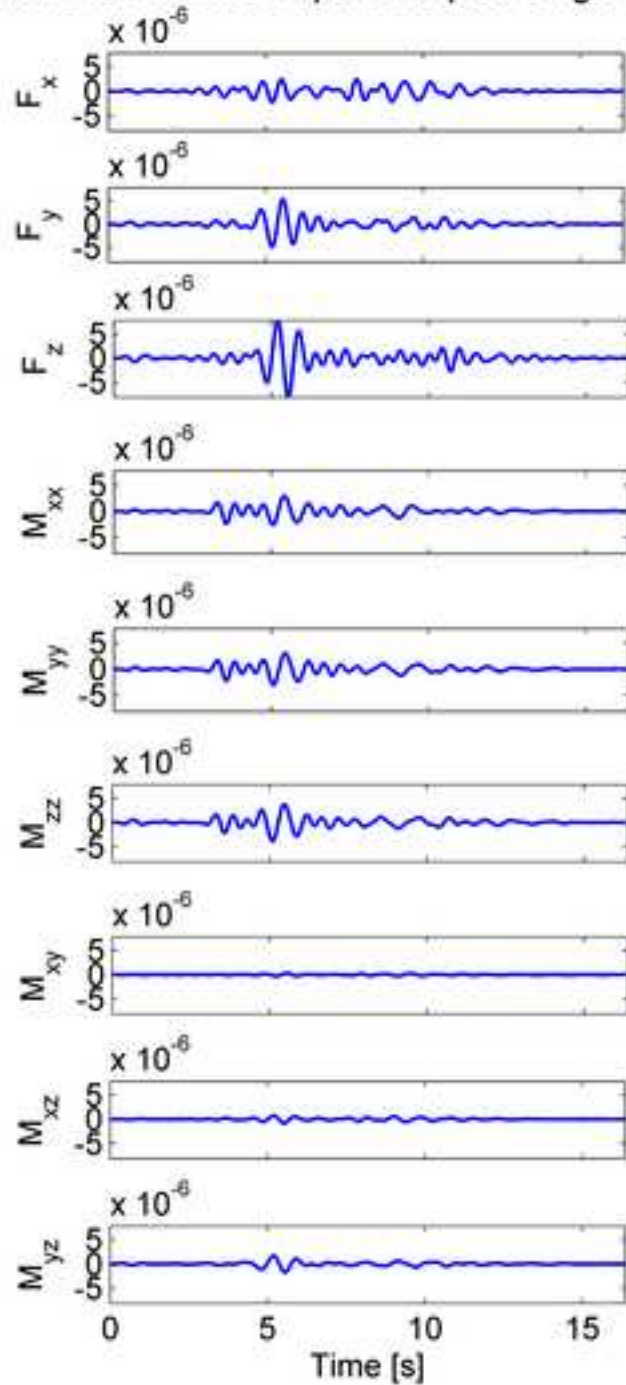


Figure 11

[Click here to download high resolution image](#)

Moment Tensor Components plus Single Forces



Moment Tensor Components

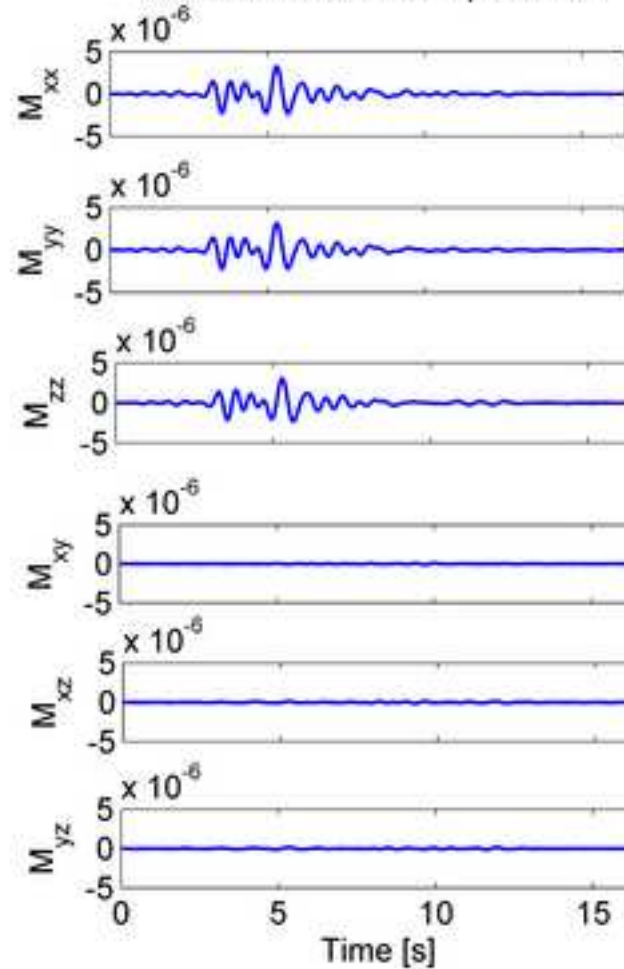


Figure 12
[Click here to download high resolution image](#)

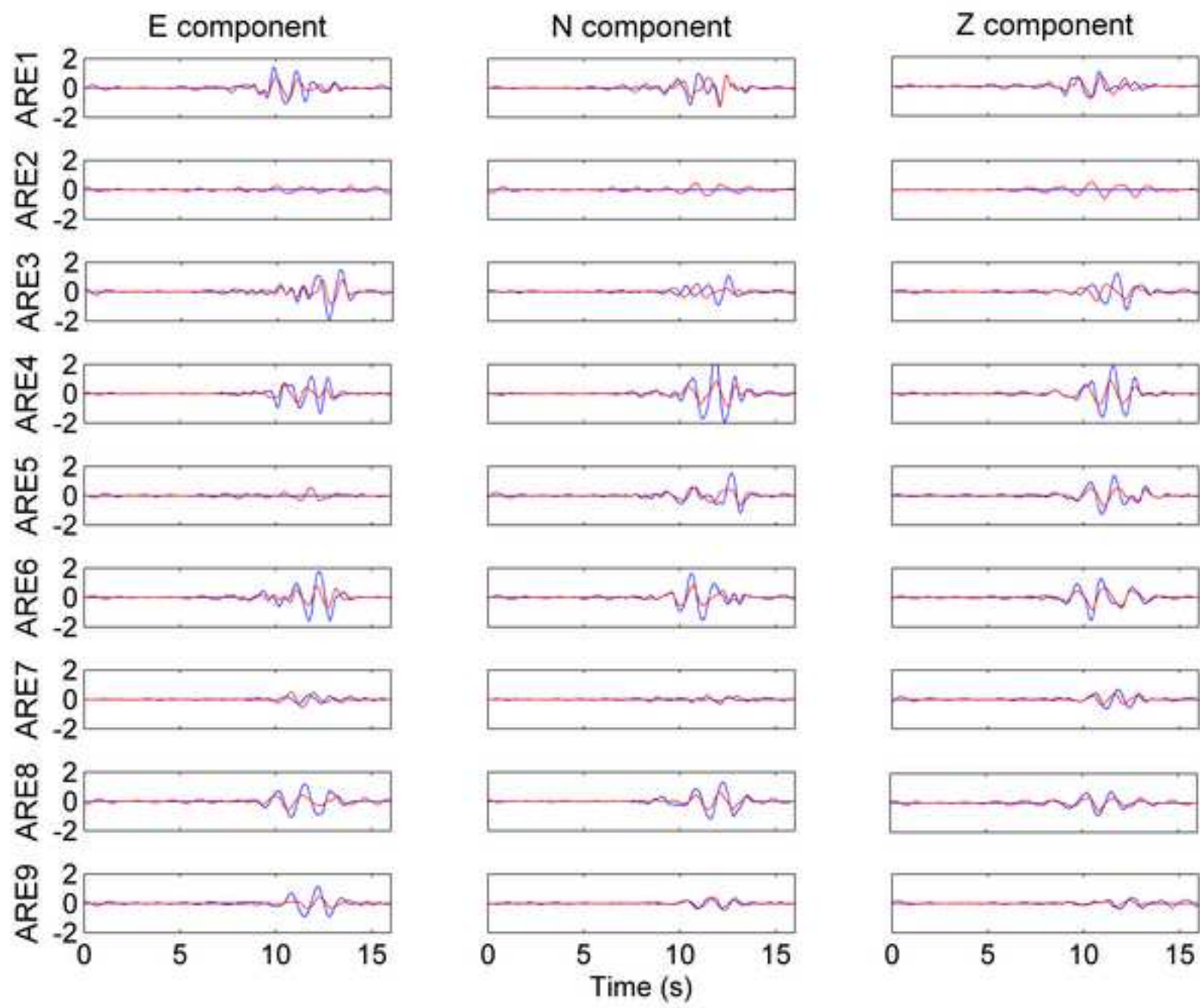


Figure 13

[Click here to download high resolution image](#)

Moment Tensor Components plus Single Forces

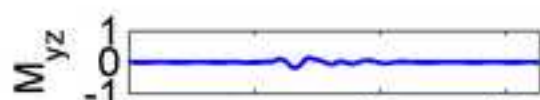
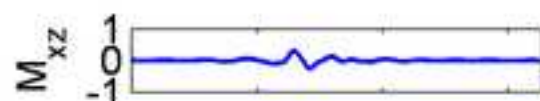


$[F]=10^9 \text{ N}$
 $[M]=10^{12} \text{ Nm}$



0 5 10 15
Time [s]

Moment Tensor Components



0 5 10 15
Time [s]

Table

[Click here to download Table: Table 1.xls](#)

Test n.	Description	S/N	Inverted components	Misfit (R)
1	data contaminated with random noise	10	MT	0.092
		10	MT + SF	0.086
2	data contaminated with random noise	2	MT	0.252
		2	MT + SF	0.226
3	data contaminated with random noise for a pure volumetric source geometry	10	MT	0.099
		10	MT + SF	0.083
4	data contaminated with random noise for a vertical crack source geometry	10	MT	0.103
		10	MT + SF	0.088
5	data contaminated with random noise for a mislocated source position	10	MT	0.097
		10	MT + SF	0.093
6	40 s long source time function		MT	0.092
			MT + SF	0.049
7	Explosion Feb 14th, 2005		MT	0.567
			MT + SF	0.418